Applied Ocean Research 176 (2026) 105317



Contents lists available at ScienceDirect

Applied Ocean Research

journal homepage: www.elsevier.com/locate/apor



Research paper



Intelligent anti-collision in multi-vessel scenarios: a spatial DPAD decision-making model via accident data-driven

Qinghua Zhu [a,b], Shenping Hu [b], Jiaxin Du [b], Yongtao Xi [b,*], Zaili Yang [c]

[a] College of Intelligent Systems Science and Engineering, Hubei Minzu University, China
[b] Merchant Marine College, Shanghai Maritime University, Shanghai, China
[c] Liverpool Logistics, Offshore and Marine (LOOM) Research Institute, Liverpool John Moores University, Liverpool, UK

ARTICLE INFO

Keywords:
Waterway transportation
Vessel intelligent anti-collision
Predicted area of danger
Adaptive decision

ABSTRACT

One of the core technologies for water transportation safety is the intelligent anti-collision technology for vessels. Although significant progress has been made in the research of intelligent anti-collision for vessels, the problem of multi-vessel adaptive anti-collision in complex waters has not been fully explored. In view of this, this paper proposes an intelligent decision-making model for multi-vessel anti-collision based on the Domain Predicted Area of Danger (DPAD). Initially, concerning the mechanisms of vessel collisions and in conjunction with the requirements of the International Regulations for Preventing Collisions at Sea (COLREGs) regarding vessel maneuvering actions, a Predicted Collision Risk Area (PCRA) model based on DPAD is constructed. Subsequently, to address the requirements for resuming navigation post-anti-collision, a threshold for resumption evaluation based on Potential Collision Risk (PCR) is proposed. Additionally, Grey Wolf Optimization (GWO) and Bézier curve techniques are employed to optimize the recovery navigation path schemes after anti-collision. Finally, by incorporating representative vessel collision cases, complex scenarios involving single-vessel and multi-vessel encounters are constructed to validate the intelligent anti-collision decision model based on DPAD, thereby achieving adaptive control of vessel avoidance maneuvers. The application results show that the spatial DPAD-based anti-collision decision model is reliable during multi-vessel encounters, producing avoidance outcomes that satisfy maritime safety requirements. This model provides a novel approach to intelligent vessel anti-collision by synergistically addressing adaptive anti-collision in spatial multi-vessel encounters.

1. Introduction

With the acceleration of globalization, waterway transportation has played a critical mode of transportation that promotes economic prosperity in the world (Li et al., 2024; Li and Yang, 2023). Vessels are crucial transportation tools in waterway transportation, and their safety is the primary concern of society. However, accidents related to vessels, such as collisions and groundings, continue to occur despite the huge efforts by the community in the past decades, resulting not only in loss of life and property damage but also causing devastating disasters to the marine environment (Tsolakis et al., 2024). According to surveys, among all factors leading to these accidents, human factors account for 80% (Kujala et al., 2009). Therefore, autonomous vessels that can reduce human involvement have become the focus of attention for people in various fields in recent years. Additionally, the advancement of artificial intelligence technology has accelerated the development of vessel automation, and the level of vessel automation is continuously improving.

Research on intelligent vessel anti-collision faces two major problems: the selection of anti-collision objects and the decision-making of anti-collision methods. In terms of avoidance objects, existing autonomous anti-collision research mainly adopts the methods of target vessel avoidance or collaborative avoidance (Zhuang et al., 2016). The safe distance for avoidance is based on the domain of vessels. However, a crucial avoidance object has been overlooked, namely, the Predicted Area of Danger (PAD) (Yu et al., 2021; Zhai et al., 2022). Accident research in collision has revealed that the essence of vessel collisions occurs when two vessels arrive in the same space at the same time. In other words, the key to vessel anti-collision is to prevent both vessels from occupying the same space simultaneously. However, the challenge of effectively describing this potential collision area has been a barrier to the application of this concept in autonomous anti-collision. Early

* Corresponding author.
E-mail address: xiyt@shmtu.edu.cn (Y. Xi).

https://doi.org/10.1016/j.apor.2026.105317
Received 7 January 2026; Received in revised form 7 August 2026; Accepted 22 October 2026
Available online 29 October 2026
0141-1187/© 2026 The Authors. Published by Elsevier Ltd. This is an open access article under the CC BY license (http://creativecommons.org/licenses/by/4.0/).

studies in geometric anti-collision found that radar plotting could be utilized to delineate potential collision zones. Consequently, several researchers have begun to explore autonomous anti-collision methodologies using PAD as the avoidance object (Higaki and Hashimoto, 2023; Liu et al., 2025). Nonetheless, the radar plotting method excessively relies on graphical techniques and cannot be transferred to electronic nautical charts, leading to a renewed suspension of the PAD avoidance principles. Fortunately, with advancements in computer technology, PAD visualization techniques have been further iterated, and they can now be embedded into electronic nautical charts (Tsou, 2016). This development provides a reliable theoretical foundation for research on PAD-based anti-collision methods. Given that PAD inherently offers advantages in directly determining avoidance parameters, it is essential to give it due attention and utilize PAD to address the intelligent anti-collision challenges in multi-vessel encounter scenarios.

As for anti-collision decisions, the principle guiding vessel anti-collision at sea is "maintaining avoidance through rudder control, with auxiliary use of propulsion," and vessels generally adopt course alteration maneuvers (i.e., changing direction, accelerating, or decelerating) (Zhou et al., 2023). These strategies are explicitly outlined in the International Regulations for Preventing Collisions at Sea (COLREGs). Consequently, vessel avoidance behaviors have remained a focal point in the decision-making processes of intelligent vessel anti-collision. Typically, a vessel's avoidance behavior encompasses several aspects: the timing of avoidance, motivation, method, magnitude, and effectiveness (Zhu et al., 2024). However, traditional geometric methods and intelligent algorithms rarely integrate all these factors into a comprehensive model for intelligent vessel anti-collision. The inclusion of these elements inevitably increases the complexity of intelligent anti-collision decision-making. Notably, the motivation, timing, and effectiveness of avoidance are often fixed based on vessel attributes (Zarzycki et al., 2025), while the method of avoidance is determined by the obligations of the giving-way vessel and the stand-on vessel as defined in the COLREGs (Lee and Park, 2024). The amplitude of evasion is the most challenging issue among these factors. It requires real-time adjustment of evasion decisions to cope with the complex and changeable navigation environment and the constantly changing dynamic characteristics of vessels during multi-vessel encounters (Zhao et al., 2024). Therefore, there is an urgent need for an evasion method with adaptive capabilities to ensure the efficiency, redundancy, and reliability of evasion.

In summary, over the years, various mathematical models and algorithms, including highly competitive machine learning and deep learning methods, have been developed to achieve intelligent vessel anti-collision. However, a review of the existing relevant literature still reveals some research gaps that need to be urgently addressed. First, the multi-target and multi-stage avoidance redundancy problem is faced by multiple vessels in complex water areas. Second, few existing studies comprehensively address the five elements (i.e., motivation, timing, mode, amplitude, and effect) of the anti-collision method. Finally, most of the existing anti-collision method verification scenarios come from artificially set or real-time scenarios obtained from AIS data, and few people use real collision accidents to verify the effectiveness of the methods.

To solve the problem of multi-ship intelligent collision avoidance decision-making in complex situations, an intelligent decision-making model for multi-ship encounter collision avoidance considering DPAD is proposed. To do so, the remainder of this paper is organized as follows. Section 2 systematically reviews the research on vessel intelligent anti-collision, summarizing the methods used in the literature, including both classical and advanced approaches (e.g., empirical learning, intelligent algorithms, and geometric methods). The problem and methods descriptions are described in Section 3 in detail. The experimental results of scenario inversion and reconstruction, as well as intelligent anti-collision decision-making for single-vessel and multi-vessel encounters, are obtained from all different encounter situations in Section 4. In Section 5, issues related to anti-collision behaviors, as well as the advantages and limitations of the method proposed in this paper, are discussed. Section 6 summarizes the paper.

2. Literature review

Anti-collision is a systematic safety measure for vessels to prevent collisions with each other. Currently, vessel anti-collision is based on geometric anti-collision. Anti-collision methods based on mathematical geometric modeling serve as the foundational logic for the entire intelligent anti-collision research process (Yu et al., 2022). In this regard, the academic community focuses on the four characteristic aspects of the anti-collision mechanism, which are motivation, timing, method, and magnitude of vessel anti-collision. Depending on the different objects of anti-collision, it can be roughly classified into geometric anti-collision based on Distance at Closest Point of Approach (DCPA) and Time to Closest Point of Approach (TCPA), geometric anti-collision based on Velocity Obstacle (VO), and geometric anti-collision based on domain (He et al., 2022; Kang et al., 2019; Szlapczynski and Szlapczynska, 2016). The following sections provide further elaboration on each of these approaches.

2.1. Geometric anti-collision based on DCPA and TCPA

Safe distance and anti-collision timing have always been critical concerns in vessel anti-collision (Zhu et al., 2023). Consequently, DCPA and TCPA have become the two primary bases for decision-making in intelligent vessel anti-collision (Wang et al., 2017; Zhen et al., 2017). However, in practical navigation, whether to use DCPA, TCPA, or a combination of both for decision-making remains a topic of intense debate. This has led to discussions on the application of fuzzy logic and neural networks in determining the timing and motivation of anti-collision actions (Ahn et al., 2012; Ohn and Namgung, 2020). Additionally, to resolve conflicts between DCPA and TCPA in decision-making, scholars have increasingly employed mathematical methods to integrate these two, or even more, parameters to assess collision risk and guide avoidance actions (Bakdi and Vanem, 2022). Although anti-collision decisions based on DCPA and TCPA have been widely praised, they lack exploration regarding the magnitude of avoidance actions.

2.2. Geometric anti-collision based on VO

The VO algorithm, originally an anti-collision method for robots, possesses the capability to judge anti-collision motivation and make avoidance decisions. Despite being an intelligent algorithm, it is built on geometric mathematical models and shares similarities with the geometric principles of vessel anti-collision. For instance, Zhang et al. (2023) proposed an improved VO method by integrating the Closest Point of Approach (CPA) model, which can be used to obtain local paths. Furthermore, the improved VO algorithm has been successively applied to intelligent vessel anti-collision (Chen et al., 2020; Huang et al., 2019). Whether in DCPA-based or VO-based anti-collision methods, the safe distance range of vessels is both critical and problematic. Given this, can the area formed by the safe distance of vessels be directly treated as the object for anti-collision? This line of thinking has promoted the emergence of domain-based anti-collision methods.

2.3. Geometric anti-collision based on the domain

The vessel domain is central to domain-based anti-collision methods and represents a significant research achievement in determining the timing of actions and safe passing distances in anti-collision behavior studies (Bakdi et al., 2021). The introduction of vessel domains has replaced the traditional roles of DCPA and TCPA in anti-collision. Currently, anti-collision methods based on vessel domains are widely

applied in intelligent anti-collision, including VO algorithms that rely on vessel domains (Liu et al., 2024). The intelligent anti-collision algorithm most closely aligned with this is the APF, as the concept of vessel domains originally draws inspiration from the repulsion fields of particles (Zhang et al., 2024). Additionally, another domain-based anti-collision method similar to vessel domains is the PAD. Unlike vessel domains, PAD is a product of radar plotting. The PAD method assumes that in an encounter situation, two vessels may simultaneously arrive at the same position, i.e., a potential collision point (Higaki and Hashimoto, 2023). Considering factors such as vessel size, measurement errors, and safe passing distances, the area derived from radar plotting is called PAD (Tam et al., 2009). Specifically, PAD incorporating an uncertain range of motion of the vessel is referred to as the Domain Predicted Area of Danger (DPAD). Anti-collision methods based on PAD take into account the motivation, timing, manner, and magnitude of anti-collision. The motivation is reflected in the existence of a PPC, the timing is reflected in the relationship between PAD size and safe distance, and the manner is reflected in the need to avoid PAD to ensure safe vessel navigation. PAD, being a product of radar plotting, inherently has the advantage of directly determining the magnitude of avoidance (Tsou, 2016).

However, compared with a vessel domain, which defines a protected safety boundary around a vessel, PAD focuses on the dangerous area generated by relative motion. Existing PAD-based studies have shown its value in identifying dangerous encounter regions and supporting the determination of avoidance amplitude. However, conventional PAD is often used as a geometric warning region or as a fixed obstacle. Its coupling with domain-based safety margins, COLREG constraints, and operational heading/rudder decisions remains insufficient.

2.4. Research gaps and contributions of this study

The above review indicates that existing geometric anti-collision methods provide different but complementary decision information. DCPA/TCPA-based methods are useful for evaluating collision risk and avoidance timing, but they provide limited guidance for determining the avoidance amplitude. VO-based methods can identify unsafe velocity or heading sets, but additional decision rules are usually required to select COLREG-compliant rudder actions. Vessel-domain methods define the protected safety space around a vessel and are effective for safe-distance assessment, but they do not directly represent the predicted dangerous area generated by encounter motion. PAD related methods focus more directly on potential collision areas and dangerous headings, but the connection between the predicted dangerous area, vessel-domain safety margin, and executable avoidance command has not been fully established.

To address this gap, this study extends PAD by incorporating the vessel-domain safety boundary and proposes the Domain Predicted Area of Danger (DPAD) as the spatial object for anti-collision decision-making. In this formulation, DPAD represents not only the predicted dangerous area of an encounter, but also the domain-based safety margin that should be avoided for safe passing. By judging the relationship between candidate headings of the own ship and the DPAD, unsafe and navigable heading intervals can be obtained. This provides a direct basis for collision-risk assessment, target prioritization, COLREG-based responsibility identification, rudder-angle selection, and subsequent route recovery in multi-vessel adaptive anti-collision.

The main contributions are as follows:

First, a DPAD-based avoidance-object formulation is established. Unlike methods that directly regard the target ship or its instantaneous domain as the avoidance object, the proposed formulation treats the encounter-specific dangerous area with a domain safety margin as the object to be avoided. This helps convert spatial collision-risk perception into a more operational heading-selection problem.

Second, a PCRA decision model is developed by coupling the vessel collision mechanism with the key elements of anti-collision behavior, including motivation, timing, method, magnitude, and effect. In multi-vessel encounters, OS–TS conflicts are prioritized according to PCR, and avoidance actions are then selected sequentially under COLREG constraints. The model therefore supports adaptive rudder-angle commands while maintaining a clear decision logic.

Finally, accident-case-based validation scenarios are constructed from representative vessel collision cases to test the proposed framework under typical single-vessel and multi-vessel encounter situations. A GWO-Bézier route recovery module is further integrated to evaluate not only collision avoidance, but also the safety and smoothness of post-avoidance route resumption.

3. Problem description and framework

3.1. Mathematical problems of anti-collision for vessels

3.1.1. Vessel encountering. A vessel collision accident can be defined in mathematical terms as follows. If vessel i is at all position points $P_i(t) = \left(x_i(t), y_i(t)\right)$ (x and y are the 2-d coordinators a vessel position, P) at $t_n \in T$ (t is the time pace), record it as $P_i = \{P_i(t_1), P_i(t_2), \ldots, P_i(t_n)\}$. Vessel j is at all position points $P_j(t) = \left(x_j(t), y_j(t)\right)$ at $t_n \in T$, record it as $P_j = \left\{P_j(t_1),\ P_j(t_2),\ \ldots,\ P_j(t_n)\right\}$. When $t_i = t_j = t, t \in T$ and $P_i(t) = P_j(t)$ are satisfied, a vessel collision occurs.

Generally, before a collision accident occurs, if both vessels maintain their courses and speeds, the collision point is predictable. As shown in Fig. 1(a), the intersection of the line representing the course of the Target Ship (TS) and the circle representing the ratio of the two vessels' speeds defines the Predicted Point of Collision (PPC). However, due to various factors such as changes in courses and speeds, multiple potential collision positions exist. The set of all these positions is denoted as $\Omega = \left\{P_{ppc}(\tau_1), P_{ppc}(\tau_2), \ldots, P_{ppc}(\tau_n)\right\}$. All of these locations constitute the set $\Omega = \left\{P_{ppc}(\tau_1), P_{ppc}(\tau_2), \ldots, P_{ppc}(\tau_n)\right\}$. Ω is called the potential collision area, and determining Ω based on the uncertain range of motion of the vessel is called DPAD. If $P_i(t) \in \Omega$, then there is a collision risk between the two vessels.

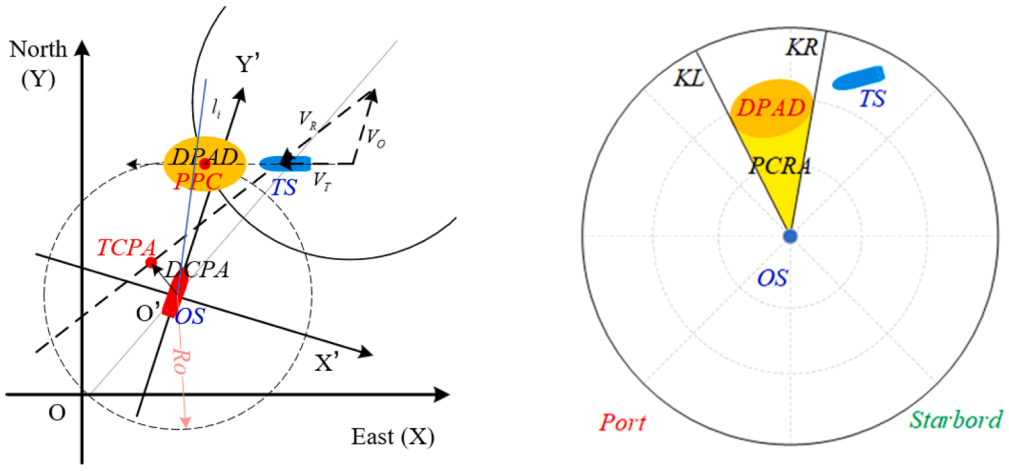
Given the mathematical definition of vessel collisions and the mechanism of collision risk formation, the essence of vessel anti-collision lies in altering courses or speeds to prevent both vessels that simultaneously enter into the DPAD. Additionally, considering the nature of vessels, the primary anti-collision measure typically involves rudder adjustments. During avoidance, the vessel's course satisfies $C_i(\theta) \in [0,\ 2\pi]$, and its speed can be represented as a vector with direction:

$$\vec{v}(t) = \left(v_x(t), v_y(t)\right) \tag{1}$$

The magnitude of the velocity can be expressed as $|\vec{v}|$.

In Fig. 1(a), any heading line $l_i(t)$ of the Own Ship (OS) $\left(x_o(t), y_o(t)\right)$ in the $C_i(t)$ direction has an intersection point $\left(x_o(t) + r\cos C_i(t), y_o + r\sin C_i(t)\right)$ with the area $\mathbb{N}$ formed by the DPAD, indicating that the TS cannot pass through the motion range of the TS safely. The set S formed by all $l_i(t)$ that produce intersection points is the PCRA, that is, $S = \left\{l(\theta) | \exists r > 0, \left(x_o + r\cos\theta, y_o + r\sin\theta\right) \in D, \theta \in [0, 2\pi]\right\}$, where $r = |\vec{v}|t$. Therefore, if $l_i(t) \notin S$, $C_i(t)$ is the safe heading.

In the radar chart centered on the OS, the PCRA can be represented by a sector area $D = \{(\rho, \theta) | \rho \le r, \alpha_0 \le \alpha \le \alpha_0 + \theta\}$ with a central angle of $\theta (0 < \theta \le 2\pi)$ and a radius of $r (0 < r)$, where α_0 and $\alpha_0 + \theta$ are the directions of KL and KR in Fig. 1(b). The PCRA range here serves as the dangerous heading area of the vessel and clearly conforms to the conventional steering avoidance principle in radar operation for anti-collision. The recommended steering here is the overall vessel steering α, but in practice, α changes dynamically, and the crew will take corresponding rudder actions based on the steering avoidance decision. Therefore, we can assume that there is a mapping relationship between $\alpha_i(t)$ and the rudder order $\Re_i(t)$, that is, $\alpha_i(t) \rightarrow \Re_i(t)$, $\Re_i(t) \in [-15, 15]$. Table 1 presents the main symbols utilized in this paper for anti-



(a) Geometric diagrams of motion parameters (b) DPAD anti-collision principle

Fig. 1. Mathematical principles of vessel anti-collision geometry.
(a) Geometric diagrams of motion parameters. (b) DPAD anti-collision principle.

Table 1
Definitions of symbols.

Symbol	Meaning	Unit/Range
a	DPAD semi-major axis	m
α	vessel overall turning avoidance amplitude	°
b	DPAD semi-minor axis	m
C	vessel heading	°
$\Re$	rudder command	°
L	vessel length	m
PCR	potential collision risk	[0, 1]
r	own ship motion circle radius	nm
θ	polar angle	rad
V	vessel speed	kn
ρ	polar radius	nm
$\mathbb{C}$	intersection area of DPAD and own ship motion circle	nm^2
$\mathbb{Z}$	area of own ship motion circle	nm^2
$\mathbb{N}$	DPAD area	nm^2

collision.

3.1.2. Vessel encounter situation based on motion parameters. To obtain the vessel's trajectory from accident reconstruction and predict the target point at time T, it is necessary to establish the motion equations of the two vessels. In a local geographic coordinate system $O-X_oY_o$ fixed to the earth, O is the origin of the geodetic coordinate system. Under this coordinate system, the position of the vessel is (x_o, y_o), the component of the vessel's motion velocity vector V in the OX_o direction is u_o, and the component in the OY_o direction is v_o. The current position of the vessel is the result of the motion of (x_o, y_o) at time t. Their motion equations are expressed as (Mou et al., 2021; Tsolakis et al., 2024):

$$\begin{cases} x_o(t) - x_o(0) = \int_0^t u_o dt \\ y_o(t) - y_o(0) = \int_0^t v_o dt \end{cases} \tag{2}$$

Given the above motion equations, let the position of the OS is $P_O(t) = (x_O(t), y_O(t))$ at time t, and the position of the TS is $P_T(t) = (x_T(t), y_T(t))$ at time t. The formula for the distance between the two vessels is as follows:

$$d(t) = \| P_O(t) - P_T(t) \|_2 \tag{3}$$

As shown in Fig. 1(a), the equations of the parameters DCPA and TCPA at any given time t, can be constructed as follows:

$$\begin{cases} DCPA(t) = d(t) \times \sin(C_R(t) - \varphi_R(t) - \pi) \\ TCPA(t) = DCPA(t)/V_R(t) \end{cases} \tag{4}$$

where, if it is on the port side then TCPA<0. If it is on the starboard side then TCPA>0. $d(t)$ is distance, V_R is the relative speed, and the direction of the relative course is C_R, φ_R is relative bearing(Tsolakis et al., 2024).

$$\begin{cases} V_R(t) = \| V_O(t) - V_T(t) \|_2 \\ \varphi_R(t) = \arctan(\hat{\mathbf{y}}^{\mathrm{T}} \widetilde{R}(z(t)) P_O(t) / \hat{\mathbf{x}}) \\ C_R(t) = C_T(t) - C_O(t) \end{cases} \tag{5}$$

where $V_O(t)$ and $V_r(t)$ are the velocities of the own ship and target ship, respectively; C_o(t) $C_O(t)$ and $C_R(t)$ are the courses of the own ship and target ship, respectively; and $\widetilde{R}(z(t))$ denotes the rotation-translation matrix.

The classification of vessel encounters is a prerequisite for premise of analyzing the anti-collision responsibility and determining the navigation mode (Guan et al., 2022). Given that this research is based on accident reconstruction to study single-vessel and multi-vessel anti-collision problems, COLREGs (International Regulations for Preventing Collisions at Sea) is an important factor that must be considered (Cui et al., 2024). COLREGs 13 to 17 delineate three distinct scenarios for the two-vessel encounter: head-on, overtaking, and crossing encounter (Zhao et al., 2022). To distinguish the different responsibilities of the give-way vessel and the stand-on vessel in cross situations conveniently, it is further divided into two different situations: port-side cross and starboard-side cross (Shi et al., 2019).

3.2. Anti-collision method based on spatial features

In view of the above problems and mathematical principles, this paper proposes an intelligent decision-making model for multi-vessel encounter anti-collision involving spatial DPAD, as shown in Fig. 2.

The details are as follows:

(1) **Situational awareness.** It is based on the vessel's dangerous encounter scenarios established from the results of accident case scenario reconstruction. First, conduct all-round TS perception beyond the visual range. Then, recognize all TSs that pose a danger to the OS. The recognition process mainly involves determining the position using the geometric method PPC, determining the DPAD range through the vessel's safe passage area, and performing numerical calculations of Potential Collision Risk (PCR) based on a Monte Carlo method. Finally,

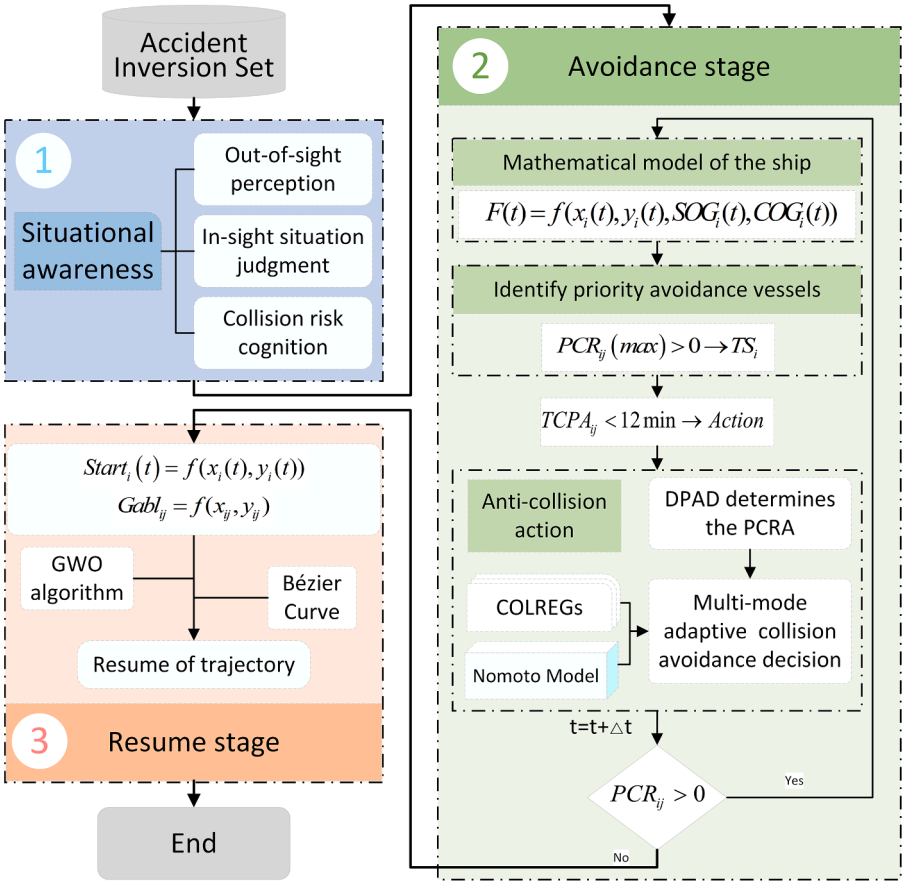


Fig. 2. The framework of Vessel intelligent anti-collision.

determine the encounter situation formed by the dangerous TSs within the visual range and the OS, and establish the responsibility relationship. The dangerous TSs are then prioritized by PCR, and the current highest-risk TS is handled first while the remaining TSs are monitored as the encounter context evolves.

(2) **Adaptive anti-collision stage.** First, based on the PCR sorting results, the TS with the largest PCR is taken as the current target for which an evasive action should be prioritized, while the remaining TSs are addressed sequentially according to their PCR and COLREG responsibilities. To ensure that the avoidance is completed before the Imminent Danger (ID) forms, the timing of the avoidance action is determined to be TCPA=12 min. Second, establish a PCRA avoidance scheme based on the DPAD between the OS and the TS. Then, establish a multimodal adaptive vessel anti-collision decision-making model considering COLREGs and vessel maneuverability. Finally, update the vessel's information and determine whether it can pass safely based on PCR.

(3) **Resumption of voyage optimization stage.** First, determine the resumption of voyage timing, starting point, and destination point based on PCR. Second, obtain the resumption of voyage path using the grey wolf algorithm. Finally, introduce the Bézier curve to smooth the resumption of voyage path to obtain the final resumption of voyage.

3.2.1. PCRA model in vessel encounter. According to the description of the evasion geometric principle in Fig. 1, in the polar coordinate system, $g_T : (\rho_T, \theta_T) \rightarrow \mathbb{R}$ and $h : (\rho_S, \theta_S) \rightarrow \mathbb{R}$ are known. If there exist (ρ_T^*, θ_T^*) and (ρ_S^*, θ_S^*) such that $g_T(\rho_T^*, \theta_T^*) = h(\rho_S^*, \theta_S^*)$, then the coordinates of PPC are $(\rho_{PPC}, \theta_{PPC})$ (Higaki and Hashimoto, 2023). Taking the PPC as the center and the uncertain range of motion of the TS as the radius to determine the DPAD, the DPAD function is constructed as follows:

$$f(a, b, \theta_{DPAD}) = ab \Big/ \sqrt{b^2\cos^2\theta_{DPAD} + a^2\sin^2\theta_{DPAD}} \tag{6}$$

where, the major semiaxis a and the minor semiaxis b of DPAD are respectively derived from the Fujii ship domain model (Fujii and Tanaka, 1971). a is the major semiaxis of the vessel domain, a = 4 L. b is the minor semiaxis of the vessel domain, b = 1.6 L. L is the length of the vessel.

According to the mathematical definition of PCRA, α_0 and $\alpha_0 + \theta$ should satisfy the following system of equations:

$$\begin{cases} \rho = g_O(\rho_O, \theta_O) \\ \rho = f(a, b, \theta_{DPAD}) \end{cases} \tag{7}$$

There is one and only one set of solutions for (ρ^*, θ^*) corresponding to the case where $(\theta_O = \alpha_0) \vee (\theta_O = \alpha_0 + \theta)$ in the equation. Here, α_0 and $\alpha_0 + \theta$ are the boundaries of the vessel's dangerous navigation area. Therefore, the heading of the evasive action should satisfy $\alpha \notin [\alpha_0, \alpha_0 + \theta]$.

However, since $\alpha \in [0°, 90°]$ and α changes in real time depending on the positional relationship between the OS and the DPAD, this is not conducive to vessel evasion and cannot achieve the desired evasion effect. In view of this, based on the investigation of multiple experienced crew members and the results of existing literature research, this study established a multimodal adaptive avoidance scheme based on the mapping relationship between heading and rudder Angle, as shown in Table 2.

It can be seen from the above description that this evasion is realized by rudder angle instructions, so the relationship between the vessel's rudder angle and heading needs to be considered. The Nomoto model

Table 2
Multimodal adaptive anti-collision scheme.

	Starboard	Port
1	$C = \{\alpha \mid \alpha \in [-30, 0]\} \rightarrow \Re\{\phi \mid \phi \in [-5, 0]\}$	$C = \{\alpha \mid \alpha \in [0, 30]\} \rightarrow \Re\{\phi \mid \phi \in [0, 5]\}$
2	$C = \{\alpha \mid \alpha \in (-60, -30]\} \rightarrow \Re\{\phi \mid \phi \in (-10, -5]\}$	$C = \{\alpha \mid \alpha \in (30, 60]\} \rightarrow \Re\{\phi \mid \phi \in (5, 10]\}$
3	$C = \{\alpha \mid \alpha \in (-90, -60]\} \rightarrow \Re\{\phi \mid \phi \in (-15, -10]\}$	$C = \{\alpha \mid \alpha \in (60, 90]\} \rightarrow \Re\{\phi \mid \phi \in (10, 15]\}$

focuses on the relationship between the vessel's turning angular velocity and the rudder angle (Ren et al., 2018). In view of this, the Nomoto model is introduced as the vessel motion model in this study. It simplifies the complex vessel maneuvering motion into a first-order linear equation by introducing the turning ability index and the following ability index.

$$T\dot{\lambda} + \lambda = K\delta \tag{8}$$

In the formula, T is the vessel's following index, K is the turning index, $\dot{\lambda}$ is the turning angular acceleration, λ is the turning angular velocity, and δ is the used rudder angle.

The response time t_κ can be obtained through the new course distance and the vessel speed V. t_κ is also the time interval for this course update.

$$t_\kappa = D_{NC} / V \tag{9}$$

where, D_{NC} is new course distance.

3.2.2. Algorithm. **(1) PCR measurement based on a Monte Carlo method.**

According to the description of the DPAD avoidance principle in Section 3.1: When the intersection $\mathbb{C}$ formed by the motion range $\mathbb{Z}$ of the OS and the DPAD occurs, it can be considered that the vessel will collide, that is, $\exists \mathbb{C} > 0$, $\mathbb{C} = \mathbb{Z} \cap \mathbb{N}$. Fig. 3 visualizes the geometric principle of PCR formation, namely the ratio of the area of the intersection region $\mathbb{C}$ between the DPAD range $\mathbb{N}$ and the movement range $\mathbb{Z}$ to the area of the movement range $\mathbb{Z}$.

Therefore, the PCR can be defined as:

$$PCR = \mathbb{C} / \mathbb{Z} \tag{10}$$

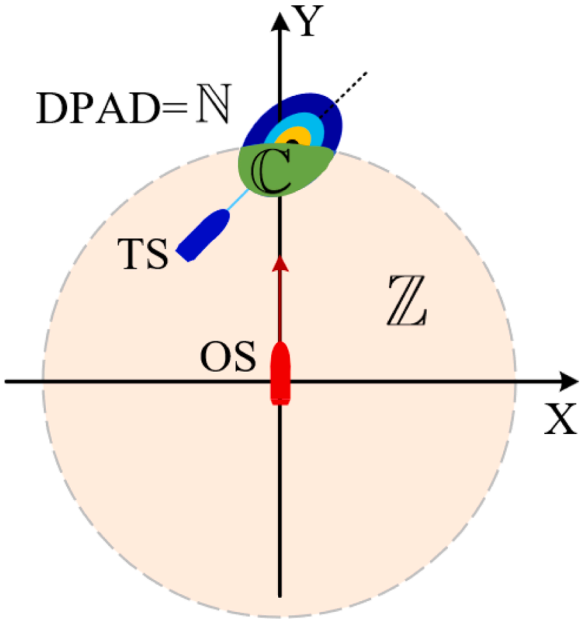


Fig. 3. The mechanism of PCR formation.

In the formula, the area of the intersecting part can be calculated by introducing a polar coordinate double integral, that is, $\mathbb{C} = \iint_D f(\rho\cos\theta, \rho\sin\theta)\rho d\rho d\theta$. The area $\mathbb{Z} = \pi r^2$ of the motion position circle, and r is the distance from the PPC to the position of the OS.

Due to the complex boundary of the integration region $\mathbb{C}$, this integration problem is difficult to solve analytically. The traditional integration methods require explicitly providing the boundary function that encloses the integration region. However, in this problem, the intersection area boundary between the OS motion circle and the DPAD cannot be pre-expressed using elementary functions, so the conventional numerical integration methods are no longer applicable. Therefore, in this paper, the Monte Carlo method is employed to approximately calculate the intersection area (Liu et al., 2006). This method is based on the law of large numbers and samples the integral region randomly. The statistical characteristics of the sample mean are used to approximate the true value of the integral. The specific calculation process is as follows:

1) Determining the range of the integral region.

Define the integral region in polar coordinates $\mathbb{N}$, so that it can completely cover the intersection area between the OS movement circle and the DPAD. This area is defined by the polar radius r and the polar angle θ. The range of values for θ is determined as follows:

$$\mathbb{N} = \{(r, \theta) \mid r_{min} \le r \le r_{max}, \theta_{min} \le \theta \le \theta_{max}\} \tag{11}$$

2) Random sampling.

Randomly generate N sample points (ρ_i, θ_i), $i = 1, 2, 3, \ldots, N$ within the integral region D. In the formal sampling, $N = 10^4$.

3) Calculating the integral estimate.

Let the indicator function $I(r_i, \theta_i)$ be defined as:

$$I(r_i, \theta_i) = \begin{cases} 1, & if(r_i, \theta_i) \in \text{Intersectionarea} \\ 0, & otherwise. \end{cases} \tag{12}$$

Then the Monte Carlo estimator A_{int} for the intersection area $\mathbb{C}$ can be expressed as:

$$\mathbb{C} = \frac{Area(\mathbb{N})}{N} \sum_{i=1}^{N} I(r_i, \theta_i) \tag{13}$$

where, $Area(\mathbb{N})$ represents the total area of the integration region D, which is equivalent to $(r_{max} - r_{min})(\theta_{max} - \theta_{min})$.

The convergence criterion adopted in this article is RSE < 0.5%.

Repeat this operation 10 times and then take the average value.

(2) GWO and Bézier Mixed Resumption Method.

Due to the evasive maneuvers, the vessel's position deviates from the planned route. Therefore, in order to ensure safe and accurate arrival at the destination, the OS should return to the planned route as soon as possible. Given the ability of bionic algorithms to handle complex situations, the GWO algorithm is selected for path optimization throughout the resumption process (Yu et al., 2022).Let the initial point of resumption be W_0 (the position of the OS when PCR first decreases to 0) and the target point be W_{n+1}. In the rasterized map, each grey wolf individual encodes a candidate recovery path as a sequence of waypoints $W = \{W_0, W_1, \ldots, W_n, W_{n+1}\}$, where $W_1, \ldots, W_n$ are the intermediate waypoints to be optimized. The position vector of each individual is represented as $X_i = \{W_1, W_2, \ldots, W_n\}$, in which each waypoint $W_j = (x_i, y_i)$ is a two-dimensional coordinate in the rasterized map.

The fitness function is designed to balance path length, safety, and smoothness:

$$F = 0.4 * L(W) + 0.4 * S(W) + 0.2 * R(W) \tag{14}$$

where $L(W) = \sum_{i=0}^{n} ||W_{i+1} - W_i||$ from $i = 0$ to n is the total path length;

$S(W) = \sum_{i=1}^{n} max(0, d_safe - d_obs(W_i))$ from$i = 1$ to n penalizes proximity to DPAD and target ship domains, with $d_{safe} = 1nm$ as the minimum clearance; and $R(W) = \sum_{i=1}^{n-1} ||\Delta\theta_i||$ from $i = 1$ to $n - 1$ penalizes large heading changes between consecutive segments, subject to a manoeuvrability constraint of delta $\Delta\theta_i <= 30^{\circ}$ per step.

Algorithm 1 outlines the GWO procedure for resumption path planning. The population size is set to M = 30, and the maximum number of iterations is $T_{\max} = 100$. The optimization terminates when the improvement of the global best fitness falls below $\epsilon = 10^{-4}$ for 20 consecutive iterations. To ensure statistical reliability and reproducibility, each scenario is independently run 30 times with a fixed random seed (seed = 42); the reported results represent the mean and standard deviation of the optimal fitness and path length across all runs.

Since the resumption path planning is carried out on a rasterized map, the generated trajectory is not smooth, which is not allowed in vessel trajectory tracking control. To solve this problem, this study introduces the Bézier curve to smooth the trajectory (Yang et al., 2024). The GWO-optimised waypoints $W_0, W_1, ..., W_n, W_{n+1}$ are directly used as the control points of the Bézier curve. The Bézier curve of order n is as follows:

$$Bezier(n,t) = \sum_{i=0}^{n} \underbrace{\binom{n}{i}}_{\text{binomialterm}} \cdot \underbrace{(1-t)^{n-i} \cdot t^{i}}_{\text{polynomialterm}} \cdot \overrightarrow{W_i} \tag{15}$$

where, $\binom{n}{i}$ represents the combination number, t is a parameter within the interval [0, 1], and $\overrightarrow{W_i}$ is an arbitrary point.

3.2.3. Single-target avoidance mode for multi-vessel encounters. Based on the above principles, the proposed model is designed for multi-vessel encounter scenarios. As shown in the Fig. 4, at each decision epoch, all detected target ships are first evaluated using PCR, and those associated with potential collision regions are ranked according to their PCR values. Once the ranking is completed, the focus of collision avoidance shifts from multiple targets to a single prioritized target. The own ship then performs COLREGs-compliant avoidance for the highest-priority target. After the own-ship state is updated, the relative states, PCR values, and target priorities are recalculated. The remaining target ships are subsequently processed one by one in the same sequential manner until no potential collision remains. Thus, the core mechanism of the entire process is dynamic target prioritization followed by sequential target-by-target avoidance in multi-vessel scenarios.

The specific procedural steps are as follows:

(1) **Perception stage**: Let the set composed of TSs is $T = \{T_i | i = 1,2, ...,n\}$. The distance between any TS T_i and the OS is D_i. The vessels that satisfy $D_i < 8$nm form the within-visual-range avoidance vessel set T' (Zhu et al., 2023). Denote it as $T' = \{T_i | D_i < 8nm, T_i \in T\}$. Calculate the PCR of all TSs in the set T and denote it as PCR_i. Find the TSs that satisfy PCR>0 and denote it as $T'' = \{T_i' | PCR_i > 0, T_i' \in T'\}$. Sort T'' according toPCR_i. The PCR_i with the largest T_i is the current avoidance object T_{avoid}.

(2) **Decision-making stage**: Based on the research conclusions of Zhu et al. (2023)and Li et al. (2022), it is assumed that the optimal timing for taking the avoidance action is when TCPA equals 12 min. Then, the avoidance action is triggered. The PCRA model serves as the evasion magnitude decision-making mechanism in this study. Let the TCPA between the OS and T_{avoid} is denoted as $TCPA = \{TCPA(i) | i = 1,2,...n\}$. When TCPA <12 min, the dangerous navigation area is obtained through the DPAD under the radar window, and then the safe recommended turning magnitude $\phi(i)$ is obtained. The rudder angle $R(i)$ helpful for evasion is obtained based on the mapping relationship between the recommended turning magnitude and the rudder angle. Finally, a systematic decision-making scheme of "motive--timing-method-magnitude-effect" is given.

(3) **Anti-collision and resumption of voyage stage**: The conversion between the rudder angle and the actual heading is completed based on the Nomoto model, and the output result is φ. Combined with the rudder angle $R(i)$ in the decision-making stage, the vessel heading update strategy under the adaptive anti-collision scheme is:

$$C_o(t+1) = \begin{cases} C_o(t) + \varphi(t) & if \quad TCPA(t) < 12\text{min} \\ C_o(t) + 0 & otherwise \end{cases} \tag{16}$$

When the PCR decreases to 0, the collision danger between the OS and the TS is eliminated, and the resumption of voyage action begins. In the resumption of voyage process, the vessel's position at the time node when the PCR first becomes 0 is taken as the starting point, and the end point of the original trajectory in the original collision scenario is taken as the target point. (He et al., 2023; Zhu et al., 2022) The GWO algorithm is used to obtain the resumption of voyage trajectory. Then, the entire resumption of voyage trajectory is smoothed using the Bézier curve.

The above four processes cover the three key processes of perception, anti-collision, and resumption of voyage in the research on intelligent vessel anti-collision decision-making. In addition, the entire process is established in open waters without considering environmental factors such as wind, current, and waves. It is worth noting that the time interval of the entire decision-making process is defined by t_κ, so as to balance the research relationship between the rudder angle and heading conversion and ensure accurate and timely control of the vessel.

Algorithm 1
GWO algorithm.

1. Initialize the gray wolf population $S_i(i = 1,2,...,n)$
2. Initialize $a, A, C, t = 0$
3. Calculate the fitness value of each gray wolf individual
4. Find the three gray wolf individuals S_α, S_β, $S_\delta$with the best fitness values
5. **While** $t < Max$
6. **For** $j = 1$ **to** M **do**
7. Update the position of the current gray wolf individual using the formula $S(t+1) = (S_1 + S_2 + S_3)/3$
8. **End For**
9. Update a, A, C
10. Calculate the fitness values of all gray wolf individuals
11. Update $S_\alpha, S_\beta, S_\delta$
12. $t = t + 1$
13. **End While**
14. Return the optimal solution S_α

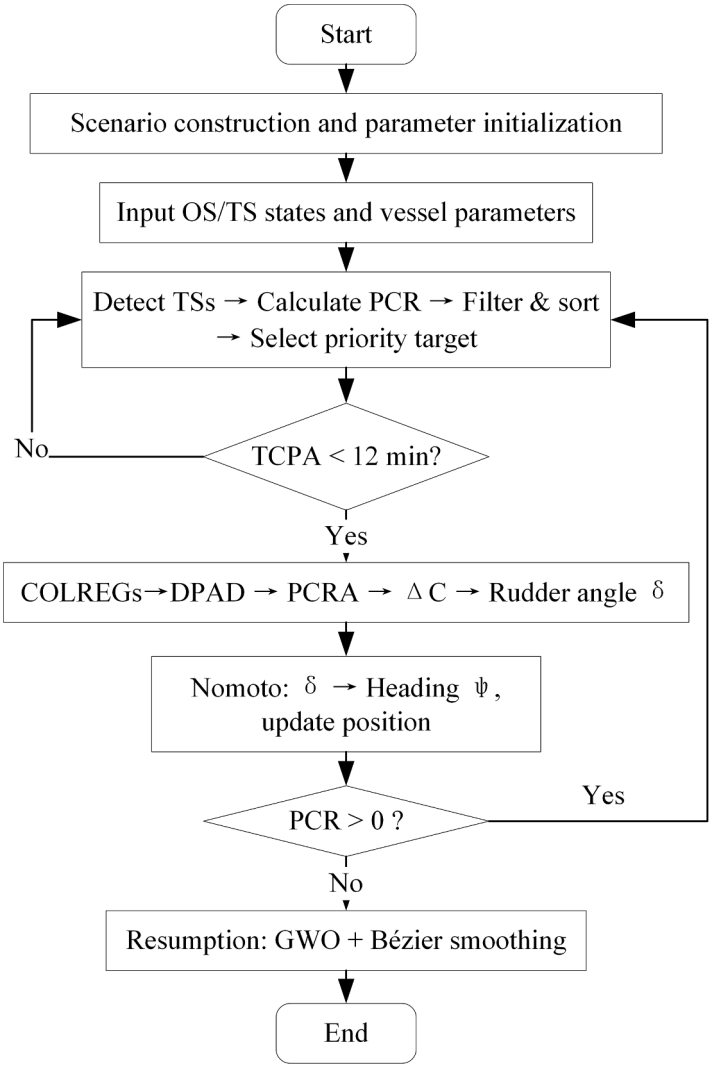


Fig. 4. Flowchart of the intelligent anti-collision decision-making model based on DPAD.

4. Result

4.1. The avoidance results of two-vessel encounters

According to statistics, vessel collisions accounted for 37% of all maritime traffic accidents annually (Pilatis et al., 2024). The objective of research on intelligent vessel anti-collision was to prevent the occurrence of vessel collision accidents. The experimental scenarios in this study are derived from collision accident cases of four different encounter situations on the website of the China Maritime Safety Administration(https://www.msa.gov.cn/). Multi-vessel encounter scenarios are constructed by aligning the pre-collision time windows in the radar coordinate system through a permutation-and-combination approach (Lee et al., 2026).

To verify the effectiveness of the research method, a collision accident that occurred in the coastal waters of eastern China was taken as the experimental scenario for a single-vessel encounter. The anti-collision process was analyzed from two perspectives: the Electronic Navigational Chart (ENC) and the Radar (RAD). Vessel type parameters are shown in Table 3. According to formula 9, the state update time is set to $t_k = 3$min.

Fig. 6(d) fully depicts the evolution of the rudder angle and course throughout the encounter process. Fig. 5(a) shows the process of establishing the experimental scenario based on the above-mentioned case, including the inversion stage and the prediction stage. Moreover, the DPAD for the current prioritized target is calculated from the encounter geometry. The advantage of using DPAD as the avoidance basis is well demonstrated in Fig. 5(d). In the radar window, one can intuitively perceive the position of the TS and the DPAD formed by its encounter situation with the OS. Taking avoidance actions according to the indication of the yellow PCRA can help avoid the TS. It is worth noting that although the PCRA gives a hint that there is also a safe navigation area on the left side, the right safe navigation area will be selected according to the requirements of COLREGs. To achieve the "early" effect required by COLREGs, the avoidance timing is determined

Table 3
Vessel type parameters.

ID	Vessel type	LPP (m)	B(m)	SOG (kn)	K'	T'	COG (°)	Initial Position [nm]	Collision Position [nm]
OS	Oil tanker	220	31.1	10.5	4.5	1.3	197	(7320.81,1769.15)	(7319.52,1764.61)
TS	Cargo vessel	86	12.5	6.4	2.07	2.06	79	(7316.26,1763.74)	(7319.52,1764.61)

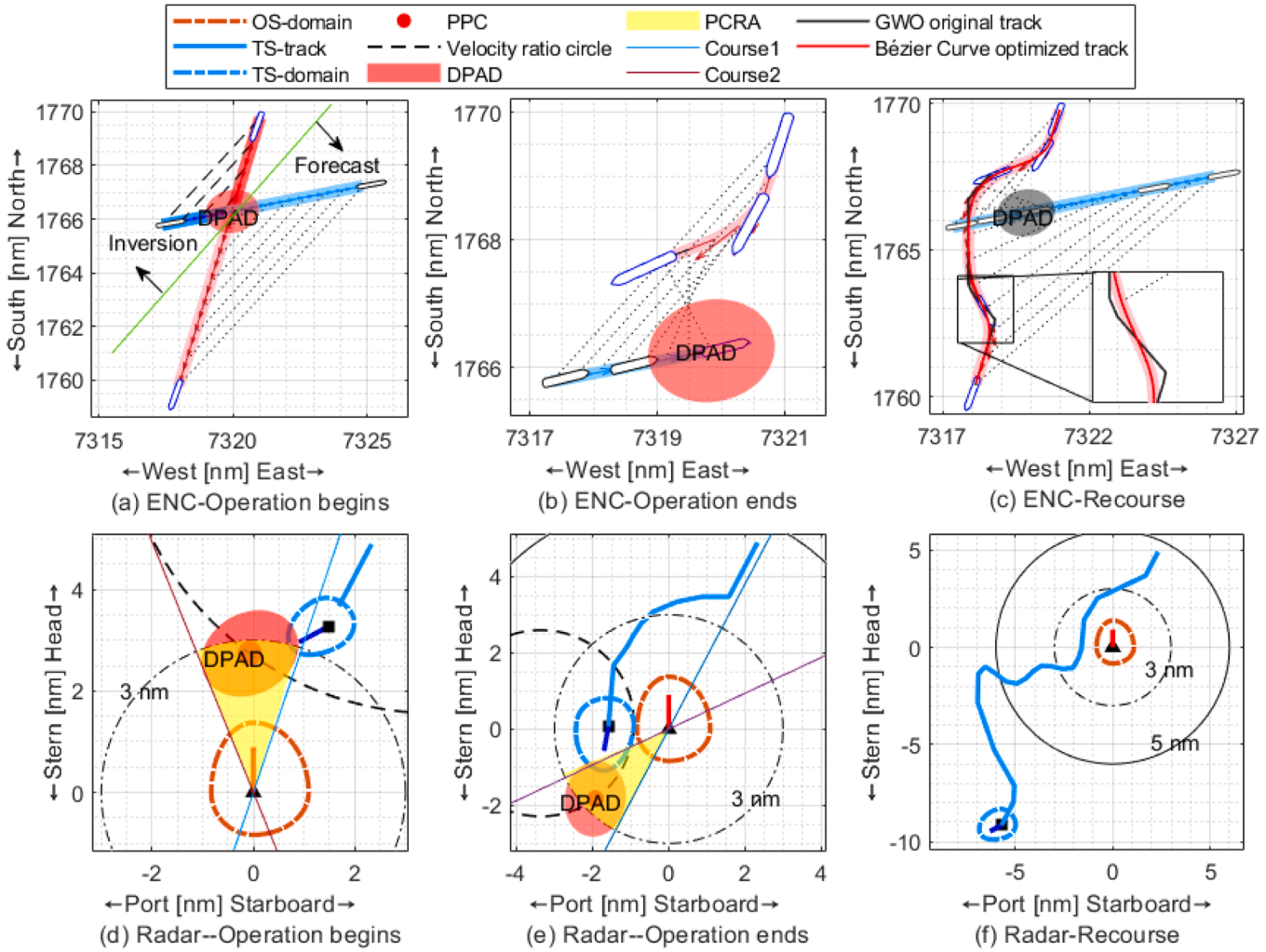


Fig. 5. The whole process of vessel avoidance from the perspective of ENC and RAD.

at TCPA=12 min, as shown in Fig. 5(c). Meanwhile, Fig. 6(c) shows that TCPA = 11.83 min, corresponding to a meeting time of 10 min. At this point, the PCR shown in Fig. 6(e) is 0.13. Fig. 5(b) records the positional relationship between the two vessels from the beginning of avoidance to the end of the avoidance action. During this period, the DPAD for this encounter phase has remained unchanged. In addition, as shown in the radar window in Fig. 5(e), when the avoidance action is triggered, the two vessels are 3.5 nm apart, and Fig. 6(b) precisely confirms this point. During the right turn avoidance of the OS, the TS has always remained outside the domain of the OS. It should be remembered that the PCRA model recommends a right turn, and the TS will appear on the left side of the OS. The safety of passing is determined based on the PCR of the two vessels, after which the resumption of voyage is initiated. At this time, the DPAD also loses its significance, and Fig. 5(c) reveals this phenomenon by filling the DPAD with gray. Because of this, in the radar window recording the entire process, the DPAD no longer exists in the resumption of voyage stage, as shown in Fig. 5(f). Moreover, the enlarged window in Fig. 5(c) shows the difference in effect between the original GWO trajectory and the optimized Bézier curve during the resumption of voyage. Obviously, the GWO trajectory optimized by the Bézier curve is smoother. Finally, Fig. 6(a) depicts the three stages of the entire evasion process: keeping course, the evasion action, and returning to the original course.

4.2. *The avoidance results of multi-vessel encounters*

Anti-collision experiments in complex encounter scenarios are also powerful means to test the effectiveness of intelligent vessel anti-collision decision-making schemes. Giving priority to avoiding the most dangerous TSs is one of the most effective ways of anti-collision in complex encounter scenarios and is also the usual practice of crew members. COLREGs clearly state the strategy of the give-way vessel turning right for avoidance. In view of this, the avoidance decision-making model of this study incorporates these two strategies and implements avoidance by determining the most dangerous vessel in the encounter situation based on PCR.

This study constructs three complex encounter scenarios based on the accident case base, as shown in Fig. 7(a), Fig. 7(e), and Fig. 7(i). Each scenario includes three different encounter situations: head-on, crossing, and overtaking. Let the OS face three scenarios in turn: Head-on & Overtaking & Crossing (HOC), Crossing & Head-on & Overtaking (CHO), and Overtaking & Crossing & Head-on (OCH). The experimental parameters for each scenario are shown in Table 4.

In Fig. 7(b), resolving the head-on situation formed with TS1 is the primary consideration for the OS's avoidance. Although TS2, which forms an overtaking situation with the OS, is the closest in distance to the OS, both the positional relationship of the DPAD and the magnitude of the PCR in Fig. 7(d) show that TS1 is the most dangerous and needs to be given priority for avoidance. In Fig. 7(d), as the avoidance action progresses, the danger between the OS and TS1 gradually decreases, while the danger with TS2 gradually increases and exceeds that of TS1. At this time, the encounter situation in the vessel's radar window is shown in Fig. 7(c), and the OS is implementing avoidance against TS2.

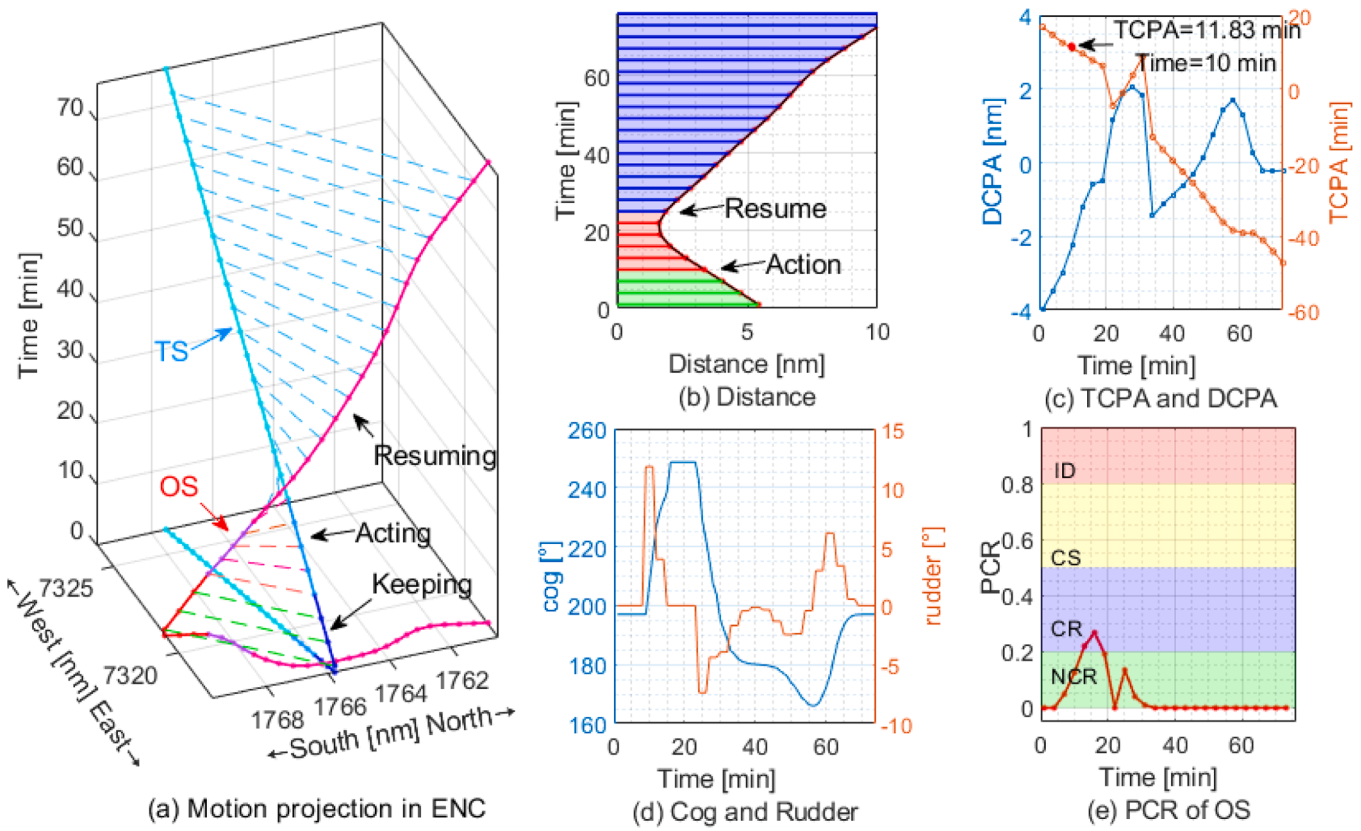


Fig. 6. Evaluation of avoidance actions in two vessel encounters.

Due to the right-turn avoidance action taken against TS1 in the previous stage, T1 is now located at the left rear of the OS with an opposite heading, and the danger with the OS is gradually eliminated. It is worth noting that at a later time, the OS forms a crossing situation with TS3, and TS3 is the give-way vessel. In this study, the same DPAD avoidance strategy is also applied to TS3, and the OS is required to maintain its course and speed. The results in Fig. 7(d) show that during the action taken by TS3, the PCRA does not appear directly in front of the OS, which further indicates the rationality of the OS's strategy of maintaining course and speed. The avoidance effects of the other two scenarios are shown in Fig. 7(f-h) and Fig. 7(j-l), where their motion trajectories are shown as dashed lines, indicating that the avoidance has been completed and is no longer considered in the current moment's avoidance actions. The results show that the method proposed in this study can handle the avoidance problems existing in the above three complex scenarios.

4.3. Sensitivity and effectiveness of the model

The effectiveness of the scheme proposed in this study during this avoidance process is significant, as evident by Fig. 8. The evaluation of multi-vessel encounter avoidance effect also includes avoidance motivation, timing, magnitude, method, and effect. The avoidance motivation is judged by PCR and the four avoidance stages. The avoidance timing depends on the TCPA value. The rationality of the avoidance magnitude and method is determined by the actual rudder angle. The most direct way to detect the avoidance effect is to observe the size of the safe distance from the TS during the avoidance process. Fig. 8 evaluates the avoidance results of three different multi-vessel encounter scenarios from the above five elements respectively.

Fig. 8(a), Fig. 8(e), Fig. 8(i), and Table 5 show that the distances between the OS and the TS during the encounter always remain outside the safe distance of 1 nm, which indicates that the entire avoidance is successful. Fig. 8(b), Fig. 8(f), and Fig. 8(g) give the trend of TCPA changes during the encounters. The area range marked in color is the trigger mechanism for the OS to take avoidance actions when $TCPA \in [-12, 12]$ min. It is possible to clearly observe the time relationship when the three TSs enter the TCPA action area. The rudder angle changes in Fig. 8(c), Fig. 8(g), Fig. 8(k), and Table 5 always remain between 15 degrees of port rudder and 15 degrees of starboard rudder, which is in line with vessel avoidance safety in open waters. In addition, this also reflects the consistency and delay between the rudder commands provided by the DPAD-based adaptive avoidance scheme in this study and the actual heading changes. In Fig. 8(d), Fig. 8(h), and Fig. 8(l), the PCR is both the basis for danger perception and the basis for determining avoidance priority. Furthermore, the change trend of PCR shows that although the avoidance action will affect the collision risk of the second dangerous vessel in the process of avoiding the most dangerous vessel. Meanwhile, Table 5 shows that in the three scenarios, the maximum value of PCR perceived by this vessel is 0.45, the collision risk between OS and TS is always in the non-collision risk (NCR) and risk of collision (CR) stages during the whole avoidance process.

The collision danger between the OS and the TS has always remained in the NCR and CR stages. This is due to the avoidance timing set in this study being TCPA=12 min and the adaptive adjustment of the avoidance magnitude in the multimodal adaptive avoidance decision model. It effectively avoids the occurrence of Critical Situation (CS) and even ID.

4.4. Comparison of avoidance effects of different avoidance targets

This study starts from the vessel collision mechanism and takes the DPAD existing in the process of collision danger formation as a fixed avoidance obstacle. As long as the DPAD is avoided during avoidance, the safety of navigation is guaranteed. In order to verify the rationality of taking DPAD as the avoidance target, this paper selects two anti-collision decisions, namely, taking the TS as the avoidance target and considering both the OS and the TS, for comparison, as shown in Fig. 9. The avoidance target of this study is not the TS itself, but the DPAD

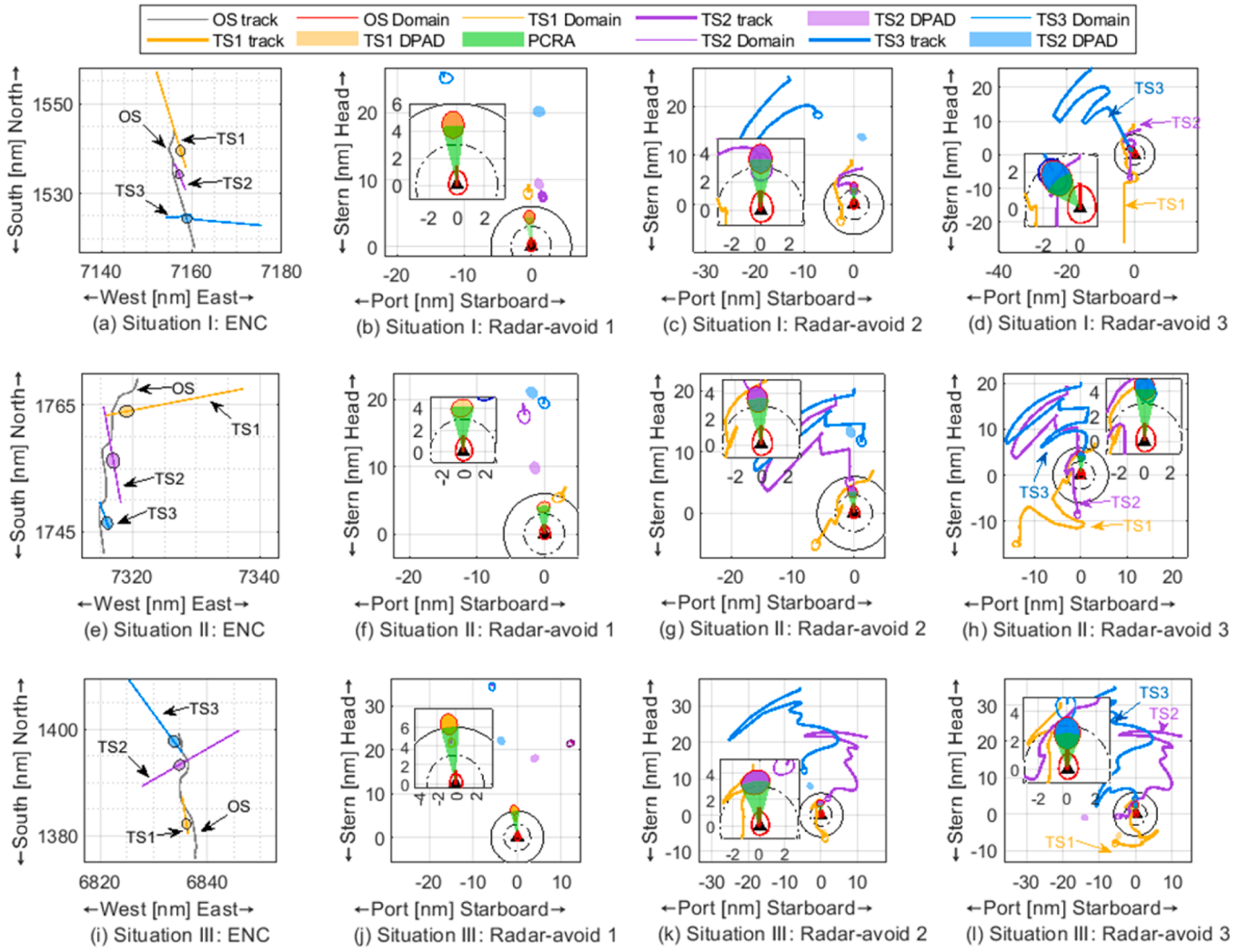


Fig. 7. The whole process of multi-vessel encounters from the perspective of ENC and RAD.

Table 4
Vessel type parameters for multi-ship collision avoidance experiment.

ID		LPP (m)	COG (°)	SOG (kn)	K'	T'	Initial Position [nm]	Target Position [nm]
HOC	OS	220	165	13.5	4.5	1.3	(7155.02, 1544.69)	(7160.69, 1517.95)
	TS1	114	343	11	0.97	0.59	(7158.71, 1535.77)	(7152.12, 1557.28)
	TS2	22	150	3	1.25	1.21	(7156.25, 1536.68)	(7158.67, 1530.72)
	TS3	86	275	10	2.07	2.06	(7175.60, 1522.91)	(7154.29, 1525.40)
CHO	OS	245	197	15	1.7	2.1	(7320.81, 1769.15)	(7314.74, 1741.57)
	TS1	127	79	10	1	1	(7315.69, 1763.32)	(7337.47, 1767.53)
	TS2	245	350	7	1.7	3.5	(7318.12, 1749.58)	(7315.43, 1764.78)
	TS3	79	160	2	1.4	2.8	(7314.79, 1749.68)	(7316.31, 1745.54)
OCH	OS	189	349	14	1.16	1.34	(6837.84, 1375.78)	(6834.59, 1399.22)
	TS1	133	2.77	4.5	2.07	1.59	(6836.50, 1380.29)	(6835.33, 1387.45)
	TS2	183	240	10	0.98	0.88	(6827.73, 1389.25)	(6846.07, 1399.78)
	TS3	160	144	8	1.9	2.53	(6825.38, 1409.23)	(6835.34, 1395.59)

between the TS and the OS, as shown in Fig. 9(a-d). Throughout the process, the DPAD remains unchanged, and it will disappear only after the danger is eliminated. In Fig. 9(e-h), typically, the TS is turned into a moving avoidance target by potential field and then avoided. Another part of people consider the mutual influence of OS and TS and introduce the vessel domain as the avoidance target (Akdag et al., 2022). This method requires that the domains of the two vessels do not touch each other during avoidance, as shown in Fig. 9(i-l).

From the avoidance results, the synergistic scheme considering the interaction between OS and TS takes the shortest time, as shown in Table 6. However, the DPAD avoidance method used in this chapter takes only 1 min longer, and the traditional APF avoidance method takes the longest time. In addition, from the perspective of encounter distance versus collision hazard, as shown in Fig. 10. Among the three different encounter methods, considering the interaction between OS and TS, the synergistic scheme sails close to the vessel domain, which ensures the safety and shortens the sailing distance to a large extent. However, this method also makes the collision danger too high and leads to a critical situation. The DPAD avoidance method used in this chapter is similar to the traditional APF method in that the minimum distance is more than

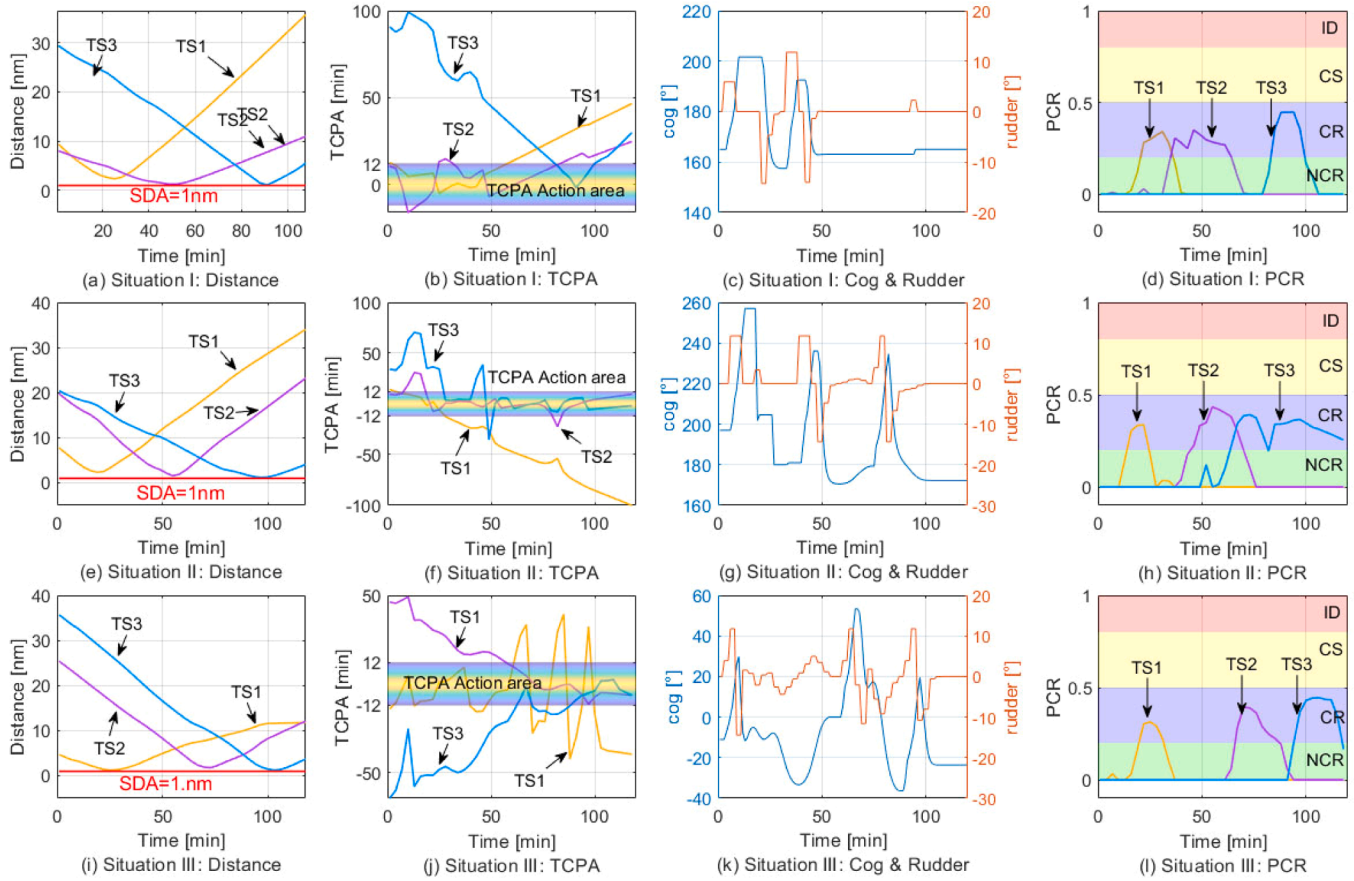


Fig. 8. Evaluation of avoidance actions in multi-vessel encounters.

Table 5
Objective safety and manoeuvring metrics for each scenario.

	Minimum CPA [nm]	Manoeuvre duration(min)	Maximum rudder angle	Maximum PCR
Situation I	1.13	92	11.77	0.45
Situation II	1.19	93	14.33	0.43
Situation III	1.22	110	14.41	0.44

2 nm. Although the DPAD avoidance method used in this chapter takes 1 min longer than the synergistic method, the safety is well guaranteed, and the maximum collision risk is 0.39 throughout the process, which never enters into a critical situation.

The advantage of using DPAD for avoidance is twofold. On the one hand, the DPAD avoidance under the radar window can directly give the required magnitude and rudder angle for avoidance, which is more conducive to establishing an adaptive anti-collision model for dealing with complex avoidance environments. On the other hand, the attributes and motion relationships of the two vessels in the encounter are placed on a fixed obstacle. This enables the vessel to quickly and accurately judge the collision danger and the primary avoidance object, and it only needs to pay attention to and avoid the DPAD during avoidance.

5. Discussion

5.1. The influence of avoidance parameters on anti-collision results

5.1.1. Timing and amplitude of avoidance. The timing and magnitude of vessel avoidance maneuvers have always been crucial in intelligent vessel anti-collision. Currently, there is a controversy regarding the timing of avoidance maneuvers, which is related to the motivation for avoidance. Some scholars believe that the formation of an ID should be avoided, advocating for taking avoidance measures during the CS stage (Yim and Park, 2022). Another group of scholars believes that the formation of a CS should be avoided as much as possible, so they advocate taking avoidance measures during the CR stage (Zhu et al., 2023). Since the stages of collision danger are different, the TCPA used to describe the avoidance timing will also vary. Additionally, in this study, the avoidance magnitude is adaptive and is determined by the mapping relationship between the PCRA and the rudder angle. Therefore, its rationality is worthy of discussion. In view of this, this study analyzes the determination of avoidance timing by selecting TCPA values of 12 min and 9 min. It further examines avoidance magnitude by testing 0.8, 1, and 1.2 times the planned rudder angle.

Fig. 11 shows the results of the analysis of the above-mentioned problems using the method of controlling variables. In the avoidance results on the ENC in Fig. 11(a) and the avoidance results in the radar window in Fig. 11(b), six different combinations of variables generate six different avoidance paths. Apparently, the avoidance maneuvers with TCPA=12 min as the avoidance timing are indeed earlier compared to those with TCPA=9 min, and Fig. 11(c) further validates this result. The PCR shows that the avoidance maneuvers with TCPA=9 min as the avoidance timing will cause the vessel to enter the CS stage, while the avoidance maneuvers with TCPA=12 min as the avoidance timing keep the PCR from entering the CS stage throughout the process. This result indicates that using TCPA=12 min as the avoidance timing is beneficial to navigation safety and meets the requirement of the "early" principle in anti-collision in COLREGs (Zhu et al., 2024). Regarding the avoidance magnitude, the avoidance trajectories of the three avoidance magnitudes in Fig. 11(a) and Fig. 11(b) do not intrude into the domain of the

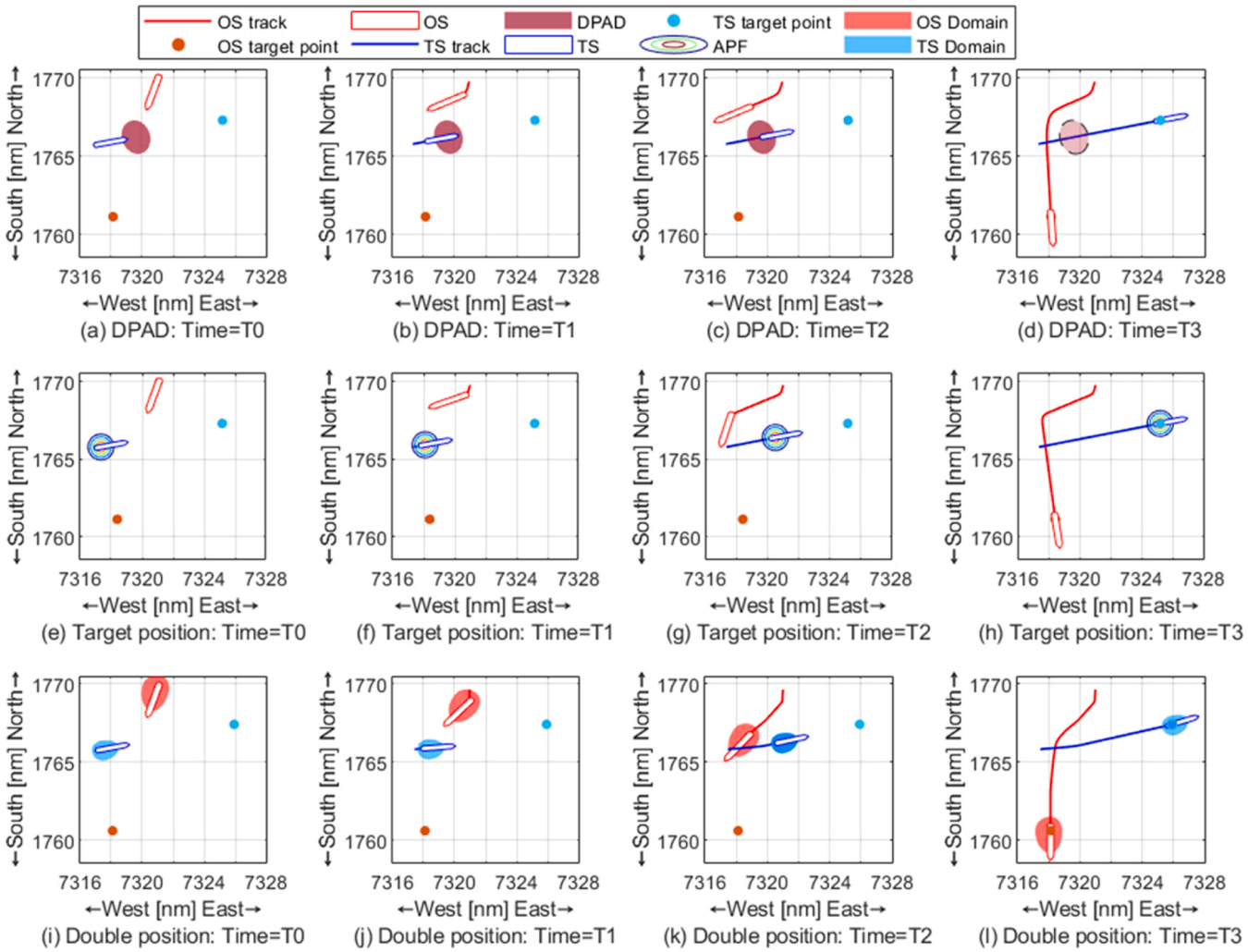


Fig. 9. Comparison of intelligent anti-collision methods considering different avoidance targets.

Table 6
The avoidance time of different methods.

ID	DPAD avoidance	Traditional avoidance	Cooperative avoidance
Speed (kn)	13.5	13.5	13.5
Voyage (nm)	10.3	10.8	10.1
Duration (min)	45	48	44

OS. The PCR of 1 time of the planned rudder angle is slightly higher than that of 0.8 times and slightly lower than that of 1.2 times the planned rudder angle. Although there are only minor differences in the avoidance paths and collision risks among the three different avoidance magnitudes, this precisely demonstrates the rationality of the mapping relationship between the PCRA and the rudder angle.

5.1.2. Basis for determining the time of resumption. Vessel resumption of voyage is another crucial stage in the intelligent vessel collision – avoidance process. However, many current studies on intelligent vessel anti-collision overlook this detail. Although some researchers have studied the timing of vessel resumption of voyage, the basis for the resumption timing remains rather unclear. Additionally, although COLREGs describe the resumption timing as "pass and clear", there is no specific definition of "clear" (Mou et al., 2021). Therefore, this study conducts comparative experimental analyses by selecting the most commonly used factors for determining the resumption timing of the vessel.

Fig. 12(a) introduces the resumption paths for each of the three conditions. The synchrone shows the following characteristics: Resumption with TCPA>12 min occurs the earliest and at the moment when the vessel-to-vessel distance is the smallest. Resumption with DCPA>2 nm occurs the latest and at the moment when the vessel-to-vessel distance is the largest. The resumption based on PCR=0 is between the other two criteria. The trend of changes in TCPA and DCPA in Fig. 12(b) indicates that at Time=22 min, it is the first time that TCPA is greater than 12 min after the implementation of the avoidance maneuver, and at Time=32 min, it is the first time that DCPA is greater than 2 nm after the implementation of the avoidance maneuver. The trend of change in PCR in Fig. 12(c) shows that at Time=25 min, PCR first decreases to 0 after the formation of danger. The radar windows in Fig. 12 (d-f) describe the positional relationship of the vessels under the three criteria. Apparently, resumption based on TCPA>12 min or DCPA>2 nm is either too early or too late. Only when PCR=0, the TS is just abeam astern of the OS. All signs indicate that PCR can be used to measure "whether passing and clearing" has been achieved, and the first time point when PCR is 0 after the formation of danger is the optimal time for resuming the voyage.

(1) Advantages of the method.

The experimental results indicate that representing collision danger by DPAD changes the anti-collision problem from target-ship avoidance to hazardous-area-targeted avoidance. Compared with methods that

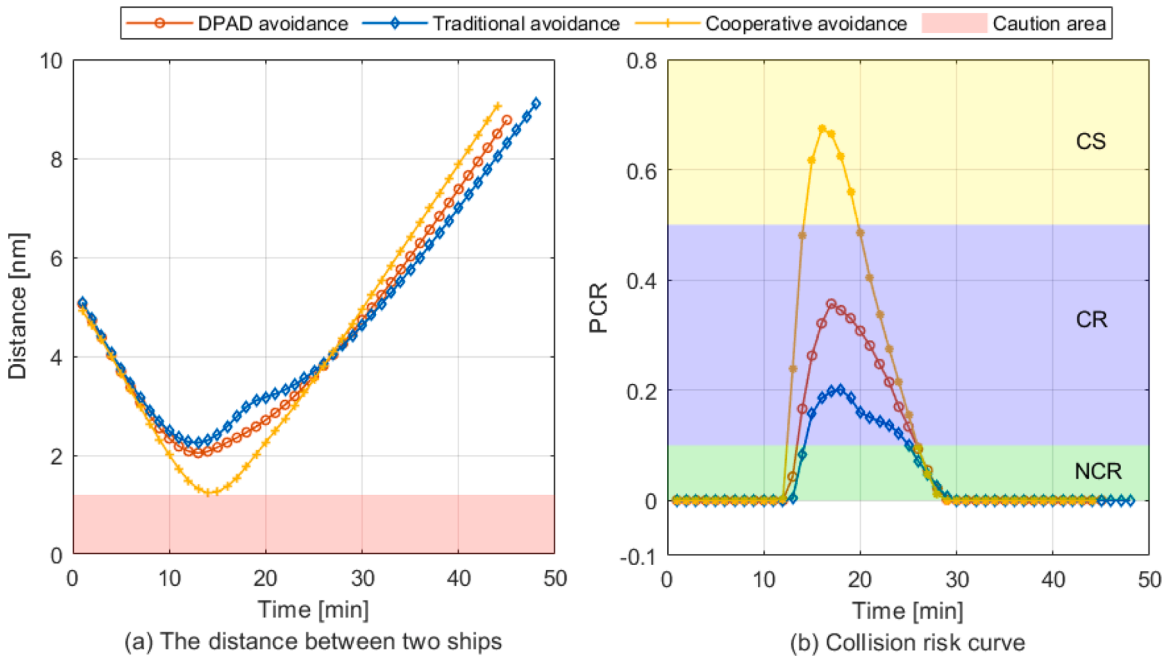


Fig. 10. The evaluation results of different avoidance methods.

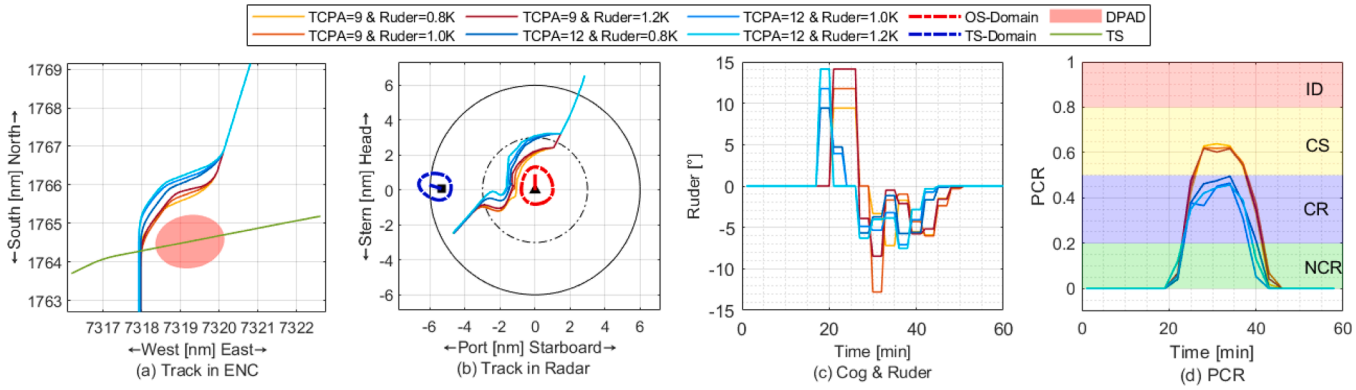


Fig. 11. Analysis of avoidance effect under different avoidance timing and different avoidance amplitude.

directly plan around the instantaneous position or predicted trajectory of the target ship, the strategy that treats DPAD as the avoidance target provides a more stable decision object in multi-vessel encounters. This helps reduce repeated small course adjustments and makes the avoidance intention clearer during the encounter process.

In the representative multi-vessel encounter scenarios constructed from accident inversion, the PCRA model generated adaptive rudder commands under the vessel motion model, and the PCR remained below 0.44 throughout the encounter. This suggests that DPAD is not only a risk-perception indicator, but also a decision constraint linking risk assessment, maneuver selection, and maneuver execution. The result also supports the design principle of taking early, large, wide, and clear actions in vessel anti-collision.

Another advantage is that the proposed framework separates anti-collision from route recovery. After the collision danger is released, the GWO-Bézier module smooths the return to the planned route and reduces abrupt changes caused by vessel inertia. In addition, the switching between radar-window DPAD-based anti-collision and ENC-based route navigation improves the practical applicability of the method in vessel anti-collision decision-support scenarios.

(2) Limitations of the method.

Nonetheless, this study still has several limitations.

First, the applicability of the proposed framework needs to be further verified in more diverse and constrained navigation scenarios. To ensure the authenticity of the anti-collision process and highlight the effectiveness of the proposed strategy, the scenarios used in this study were reconstructed from real collision accident cases. However, this also limits the range of encounter situations considered. In particular, the applicability of the proposed framework in restricted waterways, traffic separation schemes, and highly congested port environments has not yet been fully verified. In such scenarios, the feasible maneuvering space is constrained by channel boundaries, traffic lanes, separation zones, port regulations, and dense vessel interactions. In addition, environmental disturbances such as wind, current, and waves were not included in the present validation.

Second, the rudder-angle decision and vessel maneuvering dynamics require further refinement. Although the PCRA model provides adaptive rudder-angle commands, the rudder angle itself was not further optimized by an intelligent algorithm. Moreover, rudder effectiveness and actuator dynamics were simplified in the vessel motion model. To partially compensate for the time lag caused by rudder response, the rudder-command update interval was set to 3 min in this study, while the DPAD for the current prioritized target was treated as fixed within each avoidance phase. Future work will incorporate more advanced

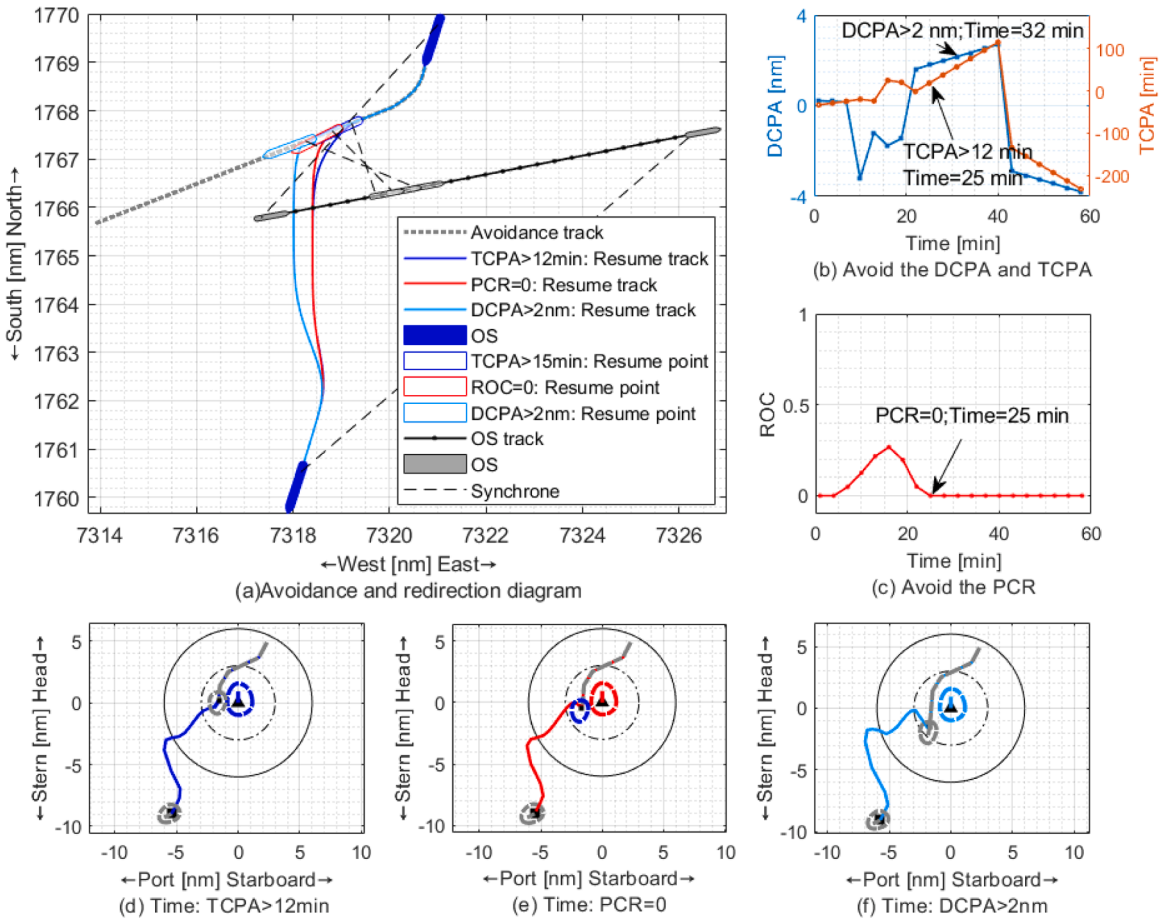


Fig. 12. The three different bases are represented in a resume.

vessel maneuvering models and intelligent optimization methods to improve the realism and control performance of the anti-collision process.

Third, the consideration of multi-vessel encounter scenarios remains incomplete. To emphasize the role of DPAD in the anti-collision decision between the OS and the TS, this study mainly focused on the anti-collision relationship between the OS and individual TSs in representative multi-vessel encounter scenarios, where the OS prioritizes conflicting targets sequentially according to PCR and COLREG responsibilities. The motion relationships and mutual influences among TSs were not explicitly considered. Future work will extend the framework to richer accident-based scenario generation and more fully coupled TS interactions, thereby further strengthening the contribution of the DPAD-guided anti-collision strategy.

6. *Conclusion*

This study proposed an intelligent decision-making model for vessel anti-collision in multi-vessel encounters involving DPAD to address the problem of intelligent vessel anti-collision in complex encounter situations. The main work included the following aspects: based on the inversion results of existing vessel collision accident cases, single-vessel encounter and multi-vessel encounter scenarios were constructed from representative encounter types. The multi-vessel encounter scenarios covered representative encounter situations. Then, considering the mechanism of vessel collision, a PCRA model was constructed based on DPAD. Vessel autonomous anti-collision was achieved according to the avoidance rudder angle provided by the PCRA model and the Nomoto model. Finally, a combined path optimization method of GWO-Bézier curve was proposed for the resumption of the voyage process. The results showed that the model proposed in this study was adaptable to complex scenarios, and DPAD became a new object of consideration in the research of intelligent vessel anti-collision. The avoidance concept proposed in this study, which takes DPAD as the object to be avoided, can provide important theoretical support for future navigation systems and intelligent decision-making of maritime autonomous surface ships (MASS).

Future work will focus on extending the proposed framework to more complex waters, including restricted waterways, dense traffic environments, and scenarios affected by wind, current, and waves. More advanced vessel maneuvering models will also be incorporated to improve the realism of anti-collision simulation. In addition, the PCRA model will be integrated with intelligent optimization, learning-based methods, and MPC-based anti-collision approaches, and will be evaluated against these methods under unified experimental conditions to further verify its effectiveness, robustness, and practical applicability.

CRediT authorship contribution statement

Qinghua Zhu: Writing – review & editing, Writing – original draft, Data curation, Conceptualization. **Shenping Hu:** Validation, Investigation, Funding acquisition. **Jiaxin Du:** Visualization, Software, Formal analysis. **Yongtao Xi:** Supervision, Resources, Project administration, Methodology. **Zaili Yang:** Writing – review & editing, Funding acquisition.

Declaration of competing interest

The authors declare that they have no known competing financial interests or personal relationships that could have appeared to influence

the work reported in this paper.

Acknowledgements

This work was supported in part by the National Natural Science Foundation of China under Grant No. 52272353 and the European Research Council (ERC) under the European Union's Horizon 2020 research and innovation programme (Grant Agreement No. 864724).

Supplementary materials

Supplementary material associated with this article can be found, in the online version, at doi:10.1016/j.apor.2026.105317.

References

Ahn, J.H., Rhee, K.P., You, Y.J., 2012. A study on the collision avoidance of a ship using neural networks and fuzzy logic. Appl. Ocean Res. 37, 162–173.
Akdag, M., Solnor, P., Johansen, T.A., 2022. Collaborative collision avoidance for maritime autonomous surface ships: a review. Ocean Eng. 250, 110920.
Bakdi, A., Glad, I.K., Vanem, E., 2021. Testbed scenario design exploiting traffic big data for autonomous ship trials under multiple conflicts with collision/grounding risks and spatio-temporal dependencies. IEEE Trans. Intell. Transp. Syst. 22, 7914–7930.
Bakdi, A., Vanem, E., 2022. Fullest COLREGs evaluation using fuzzy logic for collaborative decision-making analysis of autonomous ships in complex situations. IEEE Trans. Intell. Transp. Syst. 23, 18433–18445.
Chen, P.F., Huang, Y.M., Papadimitriou, E., Mou, J.M., van Gelder, P., 2020. An improved time discretized non-linear velocity obstacle method for multi-ship encounter detection. Ocean Eng. 196, 106718.
Cui, Z.W., Guan, W., Zhang, X.K., 2024. Collision avoidance decision-making strategy for multiple USVs based on deep reinforcement learning algorithm. Ocean Eng. 308, 118323.
Fujii, Y., Tanaka, K., 1971. Traffic capacity. J. Navig. 24 (4), 543–552.
Guan, W., Cui, Z.W., Zhang, X.K., 2022. Intelligent smart marine autonomous surface ship decision system based on improved PPO algorithm. Sensors 22, 5732.
He, Y.X., Du, Z.J., Huang, L.W., Yu, D.Q., Liu, X., 2023. Maneuver decision-making method for ship collision avoidance in chengshantou traffic separation scheme waters. Appl. Sci.-Basel 13, 8437.
He, Y.X., Liu, X., Zhang, K., Mou, J.M., Liang, Y., Zhao, X.Y., Wang, B., Huang, L.W., 2022. Dynamic adaptive intelligent navigation decision making method for multi-object situation in open water. Ocean Eng. 253, 111238.
Higaki, T., Hashimoto, H., 2023. Human-like route planning for automatic collision avoidance using generative adversarial imitation learning. Appl. Ocean Res. 138, 103620.
Huang, Y.M., Chen, L.Y., van Gelder, P., 2019. Generalized velocity obstacle algorithm for preventing ship collisions at sea. Ocean Eng. 173, 142–156.
Kang, L.J., Lu, Z.Y., Meng, Q., Gao, S., Wang, F.W., 2019. Maritime simulator based determination of minimum DCPA and TCPA in head-on ship-to-ship collision avoidance in confined waters. Transp. A 15, 1124–1144.
Kujala, P., Hänninen, M., Arola, T., Ylitalo, J., 2009. Analysis of the marine traffic safety in the gulf of Finland. Reliab. Eng. Syst. Saf. 94, 1349–1357.
Lee, H.J., Park, D.J., 2024. Collision evasive action timing for MASS using CNN-LSTM-based ship trajectory prediction in restricted area. Ocean Eng. 294, 116766.
Lee, J.-Y., Namgung, H., Kim, J.-S., 2026. Development of collision-case-based testing scenarios for validating autonomous ship collision-avoidance algorithms. Brodogradnja 77, 77204.
Li, H.H., Xing, W.B., Jiao, H., Yang, Z.L., Li, Y., 2024. Deep bi-directional information-empowered ship trajectory prediction for maritime autonomous surface ships. Transp. Res. Pt. E-Logist. Transp. Rev. 181, 103367.
Li, H.H., Yang, Z.L., 2023. Incorporation of AIS data-based machine learning into unsupervised route planning for maritime autonomous surface ships. Transp. Res. Pt. E-Logist. Transp. Rev. 176, 103171.
Li, M.X., Mou, J.M., Chen, P.F., Rong, H., Chen, L.Y., Van Gelder, P., 2022. Towards real-time ship collision risk analysis: an improved R-TCR model considering target ship motion uncertainty. Reliab. Eng. Syst. Saf. 226, 1086502.
Liu, J.J., Zhang, J.F., Zhang, M.Y., Xin, X.R., Yang, Z.L., 2025. A novel collaborative collision avoidance decision-making methodology based on potential collision areas for intelligent navigation. Ocean Eng. 318, 120126.
Liu, Q., Chen, P.F., Li, M.X., Chen, L.Y., Mou, J.M., 2024. Regional ship collision risk assessment: an integrated approach using velocity obstacle and complex network. IEEE Trans. Intell. Transp. Syst. 15, 1728–1742.
Liu, Y.S., Yong, J.H., Zhang, H., Yan, D.M., Sun, J.G., 2006. A quasi-Monte Carlo method for computing areas of point-sampled surfaces. Comput.-Aided Des. 38, 55–68.
Mou, J.M., Li, M.X., Hu, W.X., Zhang, X.H., Gong, S., Chen, P.F., He, Y.X., 2021. Mechanism of dynamic automatic collision avoidance and the optimal route in multi-ship encounter situations. J. Mar. Sci. Technol. 26, 141–158.
Ohn, S.W., Namgung, H., 2020. Interval type-2 fuzzy inference system based on closest point of approach for collision avoidance between ships. Appl. Sci.-Basel 10, 3919.
Pilatis, A.N., Pagonis, D.-N., Serris, M., Peppa, S., Kaltsas, G., 2024. A statistical analysis of ship accidents (1990-2020) focusing on collision, grounding, hull failure, and resulting hull damage. J. Mar. Sci. Eng. 12, 122.
Ren, R.Y., Zou, Z.J., Wang, Y.D., Wang, X.G., 2018. Adaptive Nomoto model used in the path following problem of ships. J. Mar. Sci. Technol. 23, 888–898.
Shi, B.H., Su, Y.X., Wang, C., Wan, L.L., Luo, Y., 2019. Study on intelligent collision avoidance and recovery path planning system for the waterjet-propelled unmanned surface vehicle. Ocean Eng. 182, 489–498.
Szlapczynski, R., Szlapczynska, J., 2016. An analysis of domain-based ship collision risk parameters. Ocean Eng. 126, 47–56.
Tam, C., Bucknall, R., Greig, A., 2009. Review of collision avoidance and path planning methods for ships in close range encounters. J. Navig. 62, 455–476.
Tsolakis, A., Negenborn, R.R., Reppa, V., Ferranti, L., 2024. Model predictive trajectory optimization and control for autonomous surface vessels considering traffic rules. IEEE Trans. Intell. Transp. Syst. 25, 9895–9908.
Tsou, M.C., 2016. Multi-target collision avoidance route planning under an ECDIS framework. Ocean Eng. 121, 268–278.
Wang, X., Liu, Z.J., Cai, Y., 2017. The ship maneuverability based collision avoidance dynamic support system in close-quarters situation. Ocean Eng. 146, 486–497.
Yang, F., Liu, J.L., Li, S.J., Hu, X.J., 2024. Minimum jerk motion planning for maritime autonomous surface ships based on Bézier curves. J. Mar. Eng. Technol. 24, 85–97.
Yim, J.B., Park, D.J., 2022. Modeling evasive action to be implemented at the minimum distance for collision avoidance in a give-way situation. Ocean Eng. 263, 112210.
Yu, H.C., Fang, Z.X., Murray, A.T., Peng, G.J., 2021. A direction-constrained space-time prism-based approach for quantifying possible multi-ship collision risks. IEEE Trans. Intell. Transp. Syst. 22, 131–141.
Yu, H.C., Murray, A.T., Fang, Z.X., Liu, J.X., Peng, G.J., Solgi, M., Zhang, W.L., 2022a. Ship path optimization that accounts for geographical traffic characteristics to increase maritime port safety. IEEE Trans. Intell. Transp. Syst. 23, 5765–5776.
Yu, J.B., Liu, G.D., Xu, J.P., Zhao, Z.Y., Chen, Z.H., Yang, M., Wang, X.Y., Bai, Y.T., 2022b. A hybrid multi-target path planning algorithm for unmanned cruise ship in an unknown obstacle environment. Sensors 22, 26.
Zarzycki, F., Gil, M., Montewka, J., Szlapczynski, R., Szlapczynska, J., 2025. Declarative ship arenas under favourable conditions. Ocean Eng. 316, 119927.
Zhai, P.Y., Zhang, Y.J., Wang, S.B., 2022. Intelligent ship collision avoidance algorithm based on DDQN with prioritized experience replay under COLREGs. J. Mar. Sci. Eng. 10, 585.
Zhang, D., Han, J.R., Wu, D., Mao, W.G., 2024. The model of ship navigation risk field for risk assessment of icebreaker convoy operations. IEEE Trans. Intell. Transp. Syst. 25, 682–696.
Zhang, K., Huang, L.W., He, Y.X., Wang, B., Chen, J.H., Tian, Y.F., Zhao, X.Y., 2023. A real-time multi-ship collision avoidance decision-making system for autonomous ships considering ship motion uncertainty. Ocean Eng. 278, 114205.
Zhao, X.Y., He, Y.X., Huang, L.W., Mou, J.M., Zhang, K., Liu, X., 2022. Intelligent collision avoidance method for ships based on COLRGEs and improved velocity obstacle algorithm. Appl. Sci.-Basel 12, 8926.
Zhao, X.Y., Huang, L.W., Zhang, K., Mou, J.M., Yu, D.Q., He, Y.X., 2024. Dynamic adaptive decision-making method for autonomous navigation of ships in coastal waters. IEEE Trans. Intell. Transp. Syst. 25, 17917–17930.
Zhen, R., Riveiro, M., Jin, Y.X., 2017. A novel analytic framework of real-time multi-vessel collision risk assessment for maritime traffic surveillance. Ocean Eng. 145, 492–501.
Zhou, Y., Daamen, W., Vellinga, T., Hoogendoorn, S.P., 2023. Ship behavior during encounters in ports and waterways based on AIS data: from theoretical definitions to empirical findings. Ocean Eng. 272, 113879.
Zhu, J.X., Gao, M., Zhang, A.M., Hu, Y.J., Zeng, X., 2022. Multi-ship encounter situation identification and analysis based on AIS data and graph complex network theory. J. Mar. Sci. Eng. 10, 21.
Zhu, Q., Xi, Y., Hu, S., Wu, J., Han, B., 2023a. Spatial-temporal analysis method of ship traffic accidents involving data field: an evidence from risk evolution of ship collision. Ocean Eng. 276, 114191.
Zhu, Q.H., Xi, Y.T., Hu, S.P., Chen, Y., 2023b. Exploring the behavior feature of complex trajectories of ships with Fourier transform processing: a case from fishing vessels. Front. Mar. Sci. 10, 1271930.
Zhu, Q.H., Xi, Y.T., Weng, J.X., Han, B., Hu, S.P., Ge, Y.E., 2024. Intelligent ship collision avoidance in maritime field: a bibliometric and systematic review. Expert Syst. Appl. 252, 124148.
Zhuang, Y.F., Sharma, S., Subudhi, B., Huang, H.B., Wan, J., 2016. Efficient collision-free path planning for autonomous underwater vehicles in dynamic environments with a hybrid optimization algorithm. Ocean Eng. 127, 190–199.